A survey of circumstellar CO emission from a sample of IRAS point sources

Nyman, L.-Å.; Booth, R.S.; Carlstrom, U.; Habing, H.J.; Heske, A.; Sahai, R.; ... ; Winnberg, A.

ASTRONOMY & ASTROPHYSICS
SUPPLEMENT SERIES

Astron. Astrophys. Suppl. Ser. **93**, 121-150 (1992)

A Survey of circumstellar CO emission from a sample of IRAS point sources

L.-Å. Nyman[1,2], R.S. Booth[1], U. Carlström[1], H.J. Habing[3], A. Heske[3,*], R. Sahai[4], R. Stark[3], W.E.C.J. van der Veen[5,**] and A. Winnberg[1]

[1] Onsala Space Observatory, Chalmers University of Technology, S-439 00 Onsala, Sweden
[2] SEST project, ESO/La Silla, Casilla 19001, Santiago 19, Chile
[3] Sterrewacht Leiden, Postbus 9513, NL-2300 RA Leiden, The Netherlands
[4] Astrophysics Dept., Chalmers University of Technology, S-412 96 Gothenburg, Sweden
[5] JCMT Unit, ROE, Blackford Hill, Edinburgh EH9 3HJ, Scotland, U.K.

Received March 18; accepted July 24,1991

Abstract. — The first results from a survey of circumstellar CO(1–0) emission are presented. The sources were selected from the IRAS point source catalog according to the IRAS color criteria described in van der Veen & Habing (1988). The sources have good quality fluxes at 12, 25, and 60 μm, flux densities larger than 20 Jy at 25 μm, and are situated more than 5° away from the Galactic plane. The survey is undertaken to study the relationship between mass loss rates, dust properties, and the evolution along the AGB.

The sample consists of 787 sources and contains both oxygen and carbon–rich stars, including Mira variables, OH/IR objects, proto–planetary nebulae, planetary nebulae, and 60 μm excess sources. So far 519 objects, situated on both the northern and the southern sky, have been observed; 163 sources were found to have circumstellar CO emission, and in 58 of these CO emission has not previously been detected.

In this paper the observed sources are presented together with some statistics, and the sensitivity and detection rate of the survey are discussed.

Key words: Stars: circumstellar matter – Stars: mass loss – Radio lines: molecular (CO) – Infrared radiation.

1. Introduction.

The IRAS point source catalog (PSC) contains 282 000 sources. It has been estimated that more than 80 000 of these are stars with circumstellar envelopes (CSE), of which many are associated with late type stars (Chester 1986). Most of them were not previously known. Van der Veen & Habing (1988) have made an attempt to study these point sources from an evolutionary point of view. They show that the IRAS color–color diagram (the logarithm of the 60/25 μm *versus* the 25/12 μm flux density ratios, F_{60}/F_{25} *versus* F_{25}/F_{12}) can be divided into ten regions where stars with different types of envelopes and at different evolutionary stages are situated (see our Fig. 1 and their Fig. 5 and Tab. 1). Stars with oxygen–rich envelopes form a sequence in the IRAS two–color diagram which has been interpreted as an evolutionary sequence of increasing mass loss rate (Olnon *et al.* 1984; Bedijn 1987; van der Veen & Habing 1988). It has also been interpreted as a sequence of increasing initial stellar masses (Epchtein *et al.* 1990) or a combination of the two (Likkel 1990). The track passes through regions II, IIIa, IIIb, and IV of van der Veen and Habing, where the envelope becomes thicker and cooler and there is also an increase in variability, in agreement with the idea that pulsation and mass loss occur simultaneously. All the other stars with dust/gas envelopes populate, however, a much larger area in the diagram. Carbon–rich stars are typically located in region VII and the upper part of IIIa, i.e. displaced towards larger F_{60}/F_{25} flux ratios, which is caused by the larger emissivity of carbon dust (Zuckerman & Dyck 1986b). There is also a large number of stars with a strong 60 μm excess (Regs. VIa and VIb), probably caused by cold dust at a large distance from the star and a lack of hot dust close to the star. The excess may suggest that there are discontinuities in the mass loss history, possibly caused by thermal pulses (Willems & de Jong 1988). Proto–planetary (PPNe) and planetary nebulae (PNe) are mostly found in regions IV and V, where stars with very cold CSEs are situated.

Send offprint requests to: L.-Å. Nyman (ESO address).
* Present address: ESTEC, PO Box 299, NL–2200 AG Noordwijk, The Netherlands.
** Present address: Columbia University, Dept. of Astronomy, 538 West 120 Street, New York, NY 10027, USA.

CO observations of CSEs have proven to be very useful to determine outflow velocities, stellar systemic velocities, and mass loss rates (e.g. van der Veen & Olofsson 1990). We have initiated a project to detect and study the CO emission from selected IRAS point sources in the different regions of the diagram by van der Veen & Habing (1988). The idea is to build up a data base of CO observations and to investigate the relationship between mass loss rates, dust properties, and the evolution along the Asymptotic Giant Branch (AGB). The sample will be observed in the CO(1–0) and (2–1) lines, and later, observations of other molecules will allow us to study the chemistry and isotope ratios of some of the envelopes.

Previous surveys of circumstellar CO emission have been based on samples of well known evolved stars (Knapp & Morris 1985), the brighter objects in the IRAS and RAFGL catalogs (Zuckerman & Dyck 1986a,b, 1989; Zuckerman *et al.* 1986; Margulis *et al.* 1990), optically bright carbon stars (Olofsson *et al.* 1987, 1988), bright 4.6 μm M giants (Wannier & Sahai 1986), unidentified IRAS carbon stars (Nguyen-Q-Rieu et al. 1987), and PNe (Huggins & Healy 1989). Our sample includes many of these sources, but in order to form a homogeneous set of data observed using the same telescopes, we intend to reobserve them all. To cover sources that are situated on both the northern and the southern sky we have used two telescopes, the 15m SEST (Swedish–ESO Submillimetre Telescope) on La Silla in Chile and the 20m telescope of Onsala Space Observatory (OSO) in Sweden. So far 519 sources have been observed in the CO(1–0) line, which is about 2/3 of the sample. These observations have been going on during the last 3 years and many new sources have been detected. With this paper we intend to present our first results, i.e. the new detections together with some statistics. The remaining observations will take at least another two years, and the final results will be presented in our next paper.

2. The IRAS sample.

The sources were selected from the IRAS point source catalog (IRAS 1985; to be named PSC). They have IRAS colors $2.5 \cdot \log(F_{25}/F_{12}) > -2$ and $2.5 \cdot \log(F_{60}/F_{25}) > -2.5$, 25 μm flux densities larger than 20 Jy, and good quality flux densities ($Q = 3$ for 12, 25, and 60 μm fluxes). To avoid confusion with CO emission from interstellar clouds, only sources situated more than 5° away from the Galactic plane were observed. All sources in region I and VIII of van der Veen & Habing (1988) are excluded. These limitations give a total number of 787 sources, of which 137 previously have been detected in CO emission. The sources are distributed in the different IRAS regions as shown in Table 1 and Figure 1a. It is clear that there are not enough sources in region IIIb, IV, VIa, and VIb for statistical studies. Many of the IRAS point sources in these regions are situated closer than 5° from the Galactic plane. We have therefore started a few follow–up observing projects which are limited to these IRAS regions, and that have less severe restrictions in Galactic latitude. In the future we will extend the entire sample to include sources closer to the Galactic plane.

3. Observations

For observational reasons our IRAS sample is divided into two parts: i) sources with $\delta > 0°$, observed with the Onsala 20m telescope, and ii) sources with $\delta < 0°$, observed with the 15m SEST. The telescope and system parameters are given in Table 2. Both telescopes were used in a dual beam switch mode with the source alternately placed in each of the two beams, a method that yields spectra with very flat baselines. The beam separation was about 11'. All intensities are given in $T_{\rm mb}$ which is the chopper wheel corrected antenna temperature, $T_{\rm A}^*$, divided by the main beam efficiencies, $\eta_{\rm mb}$, given in Table 2. The Onsala observations were made on various occasions during 1988 and 1989 using the wide and narrow band spectrometers simultaneously. The SEST observations were made on several occasions between April 1988 and March 1990. Depending on the availability of spectrometers sometimes only the narrow band, only the wide band, or both spectrometers simultaneously were used. During the data reduction the channels of the narrow band spectrometer were added 16 by 16 to give a velocity resolution of about 1.8 km s^{-1}. The typical time spent on each source (including OFF–position, calibrations, and telescope movement) was 40 to 120 minutes, and in a few cases longer. Calibration and pointing were checked daily on NGC 7027 and IRC+10216 with the Onsala telescope, and on IRC+10216, W Aql, R Scl, and IRAS 15194-5115 with the SEST. SiO masers were also used for pointing checks.

The velocity coverage of the survey is about ±650 km s^{-1}, more than enough to include Galactic objects on basis of the Galactic rotation curve. Part of the SEST observations were made with a coverage of ±110 km s^{-1}, which still is enough to include almost all Galactic stellar objects, especially because all of our sources are situated more than 5° away from the plane. During part of the SEST observations in September 1988 a faulty multiplier caused the velocity scale to be shifted by up to 10 km s^{-1}. These sources are indicated in Table 4a; they will be reobserved later.

The positions used are those of the IRAS PSC, except for objects where accurate optical positions have been measured (taken mainly from the SAO catalog). Although the IRAS PSC gives rather large errors, in practice the positions are usually accurate to within 10". The positional uncertainties together with telescope pointing errors (Tab. 2) are normally smaller than half the beamwidth

and should not prevent us from detecting a source unless it is weak ($T_A^* \leq 0.1$ K).

4. Results.

4.1. Observed sources.

The total sample consists of 787 sources (Tab. 1), of which 328 have $\delta > 0°$ and 459 $\delta < 0°$. So far 519 sources have been observed, i.e. 66 % of the sample, and 163 sources have been detected. Among these, 58 are new detections, of which 51 are situated in the southern sky and 7 in the northern sky. Figure 1a presents the IRAS two color diagram of the total sample, 1b of the observed part of the sample, 1c of the detected sources, and 1d of the non–detections. The different regions of van der Veen & Habing (1988) are indicated, as well as the evolutionary sequence for oxygen–rich stars and the black–body curve. Table 3 presents the observed part of the sample divided into IRAS regions. Table 4 lists the parameters of the observed objects and is divided into detected, tentatively detected and non–detected sources. The tentatively detected sources will later be reobserved. The CO intensities in Table 4 are given in main beam brightness temperature. The peak intensity, T_{mb}, the center velocity, v_o, and the expansion velocity, v_{exp} (half of the full line width), of the CSE were determined by fitting a parabolic or a rectangular line profile to the observed line. I_{CO} is the integrated CO intensity over the observed profile. The source identifations were mostly taken from the IRAS PSC, and sources previously detected in CO emission were found in the papers listed in the footnote of Table 4. Spectra of all detected sources are presented in Figure 2. Several sources in our sample have already been observed by others using SEST and the Onsala telescope, mainly Olofsson *et al.* (1987, 1988). These spectra were kindly made available to us.

Occasionally the spectra include CO emission from interstellar clouds situated in the line of sight. These lines are normally strong and narrow, and can easily be distinguished from circumstellar CO emission. However, if they are superposed on the circumstellar emission, they can affect the derivation of intensities and of central and expansion velocities. Sources whose spectra include interstellar emission are marked with an asterisk in the source identification in Table 4. In some of the spectra in Figure 2 the interstellar lines have been cut to better show the circumstellar emission. If the interstellar CO emission appears in the reference beam the lines have negative intensities.

4.2. Previously detected sources.

For completeness, we observed all the sources in the sample including those to which a detection of CO (1–0) emission had been reported earlier. We detected most of the latter sources, but not all (see Tab. 4b and c), mainly because their CO (1–0) emission was usually detected at a level lower than our sensitivity limit, or the sources may only have been tentatively detected. Sources detected in the CO (2–1) line are also listed as previous detections. The CO (2–1) line can be brighter than the (1–0) line because of optical depth and beam filling effects, and in such cases the (1–0) line may be too weak to be detected.

4.3. Sensitivity and detection rates.

The detection rate of the northern sources is about half that of the southern sources (23% compared with 40%, Tab. 3). This is partly due to the higher efficiency of SEST and the lower rms noise in the SEST data, but mostly due to the difference between the two samples in the number of sources with low IRAS flux densities that so far have been observed. These points will now be discussed in more detail.

4.3.1. *Telescope efficiencies.*

The estimated antenna temperature for a source smaller than the main beam is proportional to $\eta_{mb} \cdot d^2$, where d is the diameter of the telescope. The antenna temperature ratio between the SEST and Onsala telescopes for such a source would be $T_{A,SEST}/T_{A,OSO} = 0.7 \times 15^2/0.3 \times 20^2 = 1.3$. For a source with a size larger than or near that of the main beam $T_{A,SEST}/T_{A,OSO} = 0.7/0.3 = 2.3$. Since the atmospheric opacity at the SEST site is normally lower than that at the Onsala site, the SEST telescope is somewhat more sensitive than the Onsala telescope; about a factor of 1.5 for sources smaller than the main beam and more than a factor of two for more extended sources. The rms noise in the spectra are in general a factor of two lower for the SEST data compared with the Onsala data, mainly due to the unusually bad observing season 1988–1989 at Onsala. A large part of the Onsala data were taken during periods of unstable and humid weather conditions.

4.3.2. *Sources with low IRAS flux densities.*

Most sources with a 25 μm flux density larger than 40 Jy have now been observed. Those which have not been observed so far are mostly sources in which CO has been detected by others. The southern sample consists of 253 sources with $20 < F_{25} < 40$ Jy, of which 59 sources have so far been observed. The corresponding numbers for the northern sample are 158 and 114 respectively, i.e. many more weak sources have been observed. The detection rate of the Onsala sources decreases by a factor of more than two for sources with $F_{25} < 60$ Jy while it is more constant for the corresponding SEST sources, indicating that the Onsala observations are sensitivity limited below

these flux densities. It is clear that many of the weaker IRAS sources observed with the Onsala telescope need to be reobserved to increase the sensitivity and hence the detection rate.

4.4. Line profiles.

Line profiles of circumstellar CO emission from envelopes that are not resolved by the telescope beam are normally parabolic or rectangular depending on if the emission is optically thick or thin. If the envelope is resolved and the emission is optically thin, the line profile is double peaked. Almost all of our sources with spectra having a high enough signal to noise ratio to determine the line shape show parabolic or nearly parabolic line profiles, indicating optically thick CO emission. Sources with optically thin emission are normally weak, but IRAS 01159+7220 (S Cas) can be an example of an optically thin, unresolved envelope, and IRAS 11318-7256 of a resolved envelope with a double peaked profile.

Some region II objects (mostly oxygen–rich objects with thin circumstellar shells) have more sharply peaked or nearly gaussian line shapes, e.g. IRAS 02168-0312 (o Ceti), IRAS 09076+3110 (RS Cnc), and IRAS 16011+4722 (X Her). Four of our sources show peculiar line profiles: IRAS 07559-5859 is associated with the reflection nebula IC 2220 (Dachs & Isserstedt 1973; Dachs *et al.* 1978; Pesce *et al.* 1988) and has a wide CO line profile of about 70 km s^{-1} with a central peak. It has been mapped in the CO(1–0) and CO(2–1) lines and will be discussed in a separate paper. IRAS 10329-3918 (U Ant) has a double peaked line profile. It is an object with a detached CSE, discovered and discussed by Olofsson *et al.* (1990). IRAS 10491-2059 (V Hya) has an asymmetric line profile with wings. The CO emission has been mapped by Kahane *et al.* (1988) and Tsuji *et al.* (1988) and was found to originate in a region of bipolar geometry. IRAS 17047-5650 has a "normal" profile with possible weak wings. It is a compact PN with a WC11 central star, CPD-56°8032 (Rao *et al.* 1990), and has been tentatively detected in CO(2-1) by Knapp *et al.* (1989) and in CO(1–0) by Loup et al. (1990).

4.5. Sources with continuum emission.

With the observational method used, continuum emission can be measured as an offset in intensity of the baseline of the spectrum. Continuum emission was detected toward IRAS 05251-1244 at a level of 0.8 Jy and toward IRAS 21014-1133 at a level of 0.3 Jy. Both objects are identified as PNe (Tab. 6).

4.6. Sources associated with molecular outflows.

IRAS 06053-0622, IRAS 06084-0611, and IRAS 17122-2707 were found to have strong interstellar lines in their spectra, including blue or redshifted wing emission. These IRAS sources are probably recently formed stars associated with molecular outflows. The first two objects are situated in the Orion region and the third near the ρ Oph molecular cloud.

Several other sources in our sample may also be recently formed stars. They are listed in Table 6.

4.7. Non–detections.

Most of our non–detected sources have weak 25 and 60 μm flux densities, and from the relations in section 5.3 and Table 5 it would not be possible to detect them with our sensitivity limits. However, some sources have strong IRAS flux densities ($F_{25} > 100$Jy) but are not detected in CO by us. A few have been detected previously in CO in more sensitive observations (Tab. 4c), and others are associated with young objects, but there still remain several region II and IIIa objects which should have been detected. Some of them (e.g. R Cnc, U Her, IRC-10381, and X Oph) have SiO, H_2O, and/or OH masers but are not detected by us nor in the CO (1–0) observations by Margulis *et al.* (1990). It seems likely that these objects are surrounded by a shell that is either too thin or too small to produce detectable CO (1–0) emission, maybe because the mass loss has started only recently. It is possible that CO (2–1) emission could be detected in these objects (see Sect. 4.2).

5. Circumstellar CO emission in relation to the different IRAS regions.

5.1. Detections.

Table 3 presents the observed part of the sample divided into IRAS regions. As discussed above the detection rate of the SEST data is considerably higher than that of the Onsala data. However, some trends are apparent:
i) Region VII, which to a large part consists of carbon stars, has a high detection rate.
ii) Eight out of nine objects in region VIa have been detected. Even though the numbers are small, the detection probability appears to be high.
iii) The detection rate of region VIb objects is uncertain because of the small number of sources, but it is likely to be low.

5.2. EXPANSION VELOCITIES.

The average expansion velocity, v_{exp}, for sources in the different IRAS region are presented in Figure 3 and Table 5. Its one sigma deviation (Δv_{exp}) is also given in Table 5. The average expansion velocities increase as we trace through the IRAS regions from region II through IIIa to IIIb. Region VII objects have an average expansion velocity between those of IIIa and IIIb. If the expansion velocity is determined by the stellar luminosity (radiation driven outflow) this would then imply that objects in region IIIb are, on the average, more luminous than objects in region IIIa and region II. Another factor of importance could be the increase in optical depth, and thus a better coupling between gas and photons, by going from region II to IIIa. It is also possible that our sample of region IIIa stars is biased to stars more distant than those in region II.

5.3. CO INTENSITY VERSUS 60μm FLUX DENSITY.

If the 60 μm flux density and the CO intensity are both tracers of the mass loss rate (e.g. Jura 1987; Knapp & Morris 1985) there should be a relation between the two. Such a relation has been found e.g. by Olofsson *et al.* (1987) and Margulis *et al.* (1990). Figure 4 shows a plot of the logarithm of the CO intensity *versus* the logarithm of 60 μm flux density for our detected sources, divided into the the different IRAS regions. Sources with strong IRAS fluxes and CO intensities reach a maximum in CO intensity, probably because they are resolved in the CO observations and a single observation "on source" will underestimate the total CO flux. However, by limiting the 60 μm flux density range to 1000 Jy it is possible to fit a straight line with a fairly good correlation (only three sources are excluded by this criterion, IRC+10216, AFGL618, and VY CMa). The fitted line has the following parameters:

$$\log(I_{CO}) = K_{60} \cdot \log(F_{60}) + A_{60}$$

where I_{CO} is the integrated CO intensity in K kms^{-1}. The parameters are listed in Table 5. The Onsala data were multiplied by a factor of 1.3 (see Sect. 4.3.1) before being included in the fit, and the I_{CO} scale is given in SEST main beam brightness intensities. Only region II, IIIa, IIIb, VIa, and VII have enough detected objects to make a reliable fit. It can be seen that region VIa and VII objects (mainly C–stars) on the average have stronger CO emission (by a factor of 3 to 4) than region II, IIIa, and IIIb objects (mainly O–rich stars) for the same 60 μm flux density. This is also reflected in the higher detection rate of region VIa and VII objects. If there is a linear relation between the 60 μm flux and CO intensity, the slope K should be equal to one if a log–log scale is used. This value is approached by region IIIa, VIa, and VII sources, but not the others. The IRAS regions are not pure in the sense that only carbon rich stars belong to region VIa and VII and only oxygen rich ones to the other regions, instead there is a mixture of objects in all regions. This is probably reflected in our fits to region II, and especially IIIb objects, which contain few sources and have lower correlation coefficients than region IIIa and VII. A plot like Figure 4 can be used to predict the integrated CO intensities from the IRAS fluxes for different kinds of objects.

5.4. SOURCES WITH COLD CSEs AND 60 μm EXCESS SOURCES.

IRAS regions IIIb, IV, and V include stars with cool circumstellar envelopes, e.g. OH/IR objects, PPNe, and PNe. Since many recent studies have been devoted to PPNe and PNe we list all our observed sources in these regions (and also region VIa and VIb) together with identifications in Table 6. Some of the objects are included in the list of PPNe candidates by Volk & Kwok (1989) and Kwok *et al.* (1989), and several objects are young PNe which have also been searched for OH maser emission by Zijlstra *et al.* (1989).

Many of the CO spectra of objects in these regions include strong, narrow, emission features suggesting that the lines are of interstellar origin. A few spectra include weak, narrow lines, and it is difficult to determine if they are interstellar or circumstellar. These sources will be mapped to determine whether the CO emission is extended (interstellar) or associated with the IRAS source.

Region VIa and VIb sources are objects with a 60 μm excess, indicating that cool dust is present, but warm dust is lacking. Willems & de Jong (1988) suggest that this absence is caused by discontinuities in the mass loss history, possibly due to thermal pulses. This picture is also supported by the observations of double peaked CO line profiles and by CO maps that indicate a large inner radius of the circumstellar envelopes of some of these objects (Olofsson *et al.* 1990).

Most of the region VIa sources have already been detected in CO by Olofsson *et al.* (1987, 1988). Only one region VIb object was detected, IRAS 16105-4205. It has been identified as an OH/IR object (Gaylard *et al.* 1989) and has previously been detected in CO by Zuckerman *et al.* (1986). We have made a five point CO map showing that the emission is not extended with respect to the beam. This object also has an SiO maser (Nyman, priv. comm.).

6. Conclusions and future work.

We have initiated a survey of circumstellar CO emission from a sample of 787 IRAS point sources, mainly selected using the IRAS color criteria given in van der Veen &

Habing (1988). So far 519 sources, situated on both the northern and the southern sky, have been observed in the CO (1–0) line. 163 sources have been detected of which 58 are new detections. A correlation between the integrated CO intensity and the IRAS 60 μm flux was found, supporting the idea that both are tracers of the mass loss rate. Sources belonging to region VIa and VII of van der Veen & Habing (1988), which to a significant fraction consist of C–stars, have, on the average, the highest integrated CO intensities and the highest detection rate. The average expansion velocities of the CSEs increase as we go from region II through IIIa to IIIb, suggesting a corresponding increase in stellar luminosity. Two objects, both PNe, were found to have continuum emission at 115 GHz, four objects have peculiar line profiles, and several objects were found to be associated with young stellar objects. A few sources with high IRAS flux densities, some of them associated with SiO, H_2O, and OH masers, were not detected by us, suggesting that their envelope is either too thin or too small to produce detectable CO emission, maybe because the mass loss has started only recently.

In the future our IRAS sample will be extended to include sources closer to the Galactic plane; CO (2–1) observations will be made, and selected sources will be mapped and studied in other molecules. Near infrared photometry of a large part of the sample has been performed (Fouqué *et al.*, this issue, p. 151), which will help us to determine bolometric fluxes, distances, and also to find out which sources are oxygen or carbon–rich (Epchtein *et al.* 1990). We will determine mass loss rates from the CO (1–0) and (2–1) observations, and compare them with dust properties and the evolutionary status of the objects. Our next paper will present the remaining CO (1–0) and the CO (2–1) observations.

Acknowledgements.

We are grateful to Hans Olofsson for a careful reading of the manuscript and for kindly providing us with spectra obtained by him at SEST and Onsala. SEST is operated jointly by ESO and the Swedish National Facility for Radio Astronomy, Onsala Space Observatory at Chalmers University of Technology.

References

Arquilla R., Leahy D.A., Kwok S. 1986, MNRAS, 220, 125

Bedijn P.J. 1987, A&A 186, 136

Beichman C.A., Myers P.C., Emerson J.P., Harris S., Mathieu R., Benson P.J., Jennings R.E. 1986, ApJ 307, 337

Cernicharo J., Guélin M., Martín–Pintado J., Peñalver J., Mauersberger R. 1989, A&A, 222, L1

Chester T. 1986, In: Israel, F.P. Ed. Light on Dark Matter. Reidel, Dordrecht, p.3

Cohen M., Schwartz R.D. 1984, AJ 89, 277

Dachs J., Isserstedt J. 1973, A&A 23, 241

Dachs J., Isserstedt J., Rahe J. 1978, A&A 63, 353

Deguchi S., Nakada Y., Sahai R. 1990, A&A 230, 339

Epchtein N., Le Bertre T., Lepine J.R.D. 1990, A&A 227, 82

Gaylard M.J., West M.E., Whitelock P.A., Cohen R.J. 1989, MNRAS, 236 247

Heske A., Forveille T., Omont A., van der Veen W.E.C.J., Habing H.J. 1990, A&A 239, 173

Hu J.Y., de Jong T., Slijkhuis S. 1990, In: Mennessier, M.O., Omont, A. (Eds.) From Miras to Planetary Nebulae: Which path for Stellar Evolution. Editions Frontieres, p.487

Hu J.Y., The P.S., de Winter D. 1989, A&A 208, 213

Hrivnak B.J., Kwok S., Volk K.M. 1988, ApJ 331, 832

Huggins P.J., Healey A.P. 1989, ApJ 346, 201

IRAS, Point Source Catalog 1985, US Government Publication Office

Jura M. 1987, ApJ 313, 743

Kahane C., Maizels C., Jura M. 1988, ApJ 328, L25

Knapp G.R. 1986, ApJ 311, 731

Knapp G.R., Morris M. 1985, ApJ 292, 640

Knapp G.R., Phillips T.G., Leighton R.B., Lo K.Y., Wannier P.G., Wootten H.A., Huggins P.J. 1982, ApJ 252, 616

Knapp G.R., Sutin B.M., Phillips T.G., Ellison B.N., Keene J.B., Leighton R.B., Masson C.R., Steiger W., Veidt B., Young K. 1989, ApJ 336, 822

Kwok S., Volk K.M., Hrivnak B.J. 1989, ApJ 345, L51

Lambert D.L., Gustafsson B., Eriksson K., Hinkle K.H. 1986, A&AS 62, 373

Leahy D.A., Kwok S., Arquilla R.A. 1987, ApJ 320, 825

Likkel L. 1990, In: Mennessier, M.O., Omont, A. (Eds.) From Miras to Planetary Nebulae: Which path for Stellar Evolution. Editions Frontieres, p.258

Likkel L., Omont A., Morris M., Forveille T. 1987, A&A 173, L11

Lindqvist M., Nyman L.–Å., Olofsson H., Winnberg A. 1988, A&A 205, L15

Loup C., Forveille T., Nyman L.–Å., Omont A. 1990, A&A 227, L29

Margulis M., Van Blerkom D.J., Snell R.L., Kleinmann S.G. 1990, ApJ 361, 673

Menzies J.W., Wolstencroft R.D. 1990, MNRAS 247, 177

Nquyen–Q–Rieu Epchtein N., Truong–Bach Cohen M. 1987, A&A 180, 117

Olnon F.M., Baud B., Habing H.J., de Jong T., Harris S., Pottasch S.R. 1984, ApJ 278, L41

Olofsson H., Eriksson K., Gustafsson B. 1987, A&A 183, L13

Olofsson H., Eriksson K., Gustafsson B. 1988, A&A 196, L1

Olofsson H., Carlström U., Eriksson K., Gustafsson B., Willson, L.A. 1990, A&A 230, L13
Pesce E.P., Stencel R.E., Doggett J., Walter F.M., Dachs J., Whitelock P.A., Mundt R. 1988, In: ESA SP–281, A Decade of UV Astronomy With the IUE Satellite. Vol 1, p. 253
Rao N.K., Giridhar S., Nandy K. 1990, A&A 234, 410
Sopka R.J., Olofsson H., Johansson L.E.B., Nguyen–Q–Rieu, Zuckerman, B. 1989 A&A 210, 78
te Lintel Hekkert P., Habing H.J., Caswell J.L., Norris R.P., Haynes R.F. 1988, A&A 202, L19
te Lintel Hekkert P., Versteege–Hensel H.A., Habing H.J., Wiertz M. 1989, A&AS 78, 399
Tsuji T., Unno W., Kaifu N., Izumiura H., Ukita N., Cho S., Koyama K. 1988, ApJ 327, L23
Wannier P.G., Sahai R. 1986, ApJ 311, 335
van der Veen W.E.C.J., Habing H.J. 1988, A&A 194, 125
van der Veen W.E.C.J., Olofsson H. 1990, In: Mennessier M.O., Omont A. (Eds.) From Miras to Planetary Nebulae: Which path for Stellar Evolution. Editions Frontieres, p.139
Willems F.J., de Jong T. 1988, A&A 196, 173
Volk K.M., Kwok S. 1989, ApJ 342, 345
Woodsworth A.W., Kwok S., Chan S.J. 1990, ApJ 228, 503
Zijlstra A.A., te Lintel Hekkert P., Pottasch S.R., Caswell J.L., Ratag M., Habing H.J. 1989, A&A 217, 157
Zuckerman B., Dyck H.M. 1986a, ApJ 304, 394
Zuckerman B., Dyck H.M. 1986b, ApJ 311, 345
Zuckerman B., Dyck H.M., Claussen M.J. 1986, ApJ 304, 401
Zuckerman B., Dyck H.M. 1989, A&A 209, 119

TABLE 1. *The IRAS sample.*

Region	II	IIIa	IIIb	IV	V	VIa	VIb	VII	Total
No of sources	147	394	32	15	54	9	7	129	787

TABLE 2. *Telescope and observational parameters at 115 GHz.*

	Onsala	SEST
Diameter	20m	15m
η_{mb}	0.3	0.7
θ_{FWHM}	33"	45"
Pointing	3" rms	4" rms
Receiver	SIS receiver	Schottky receiver
$T_{sys}^{(1)}$	500–1000 K	400–1000 K
Spectrometers	2 Filterbanks	2 AOS
Frequency coverage/ channel separation	512 MHz/1 MHz 64 MHz/0.25 MHz	500 MHz/0.7 MHz 86 MHz/43 kHz
Velocity coverage/ channel separation	$\pm$666/2.6 kms^{-1} $\pm$83/0.65 kms^{-1}	$\pm$650/1.8 kms^{-1} $\pm$112/0.11 kms^{-1}

(1) Including the contribution from the atmosphere and calculated as equivalent system temperature outside the atmosphere. The variations are due to different elevations and weather conditions.

TABLE 3. *Observed part of sample.*

	Observed			Onsala			SEST		
Region	Total	Det.	%	Total	Det.	%	Total	Det.	%
II	100	19	19	50	8	16	50	11	22
IIIa	229	67	29	127	26	21	102	41	40
IIIb	28	9	32	10	3	30	18	6	33
IV	13	3	23	6	1	17	7	2	29
V	46	4	9	19	1	5	27	3	11
VIa	9	8	89	5	4	80	4	4	100
VIb	7	1	14	3	0	0	4	1	25
VII	87	52	60	44	19	43	43	33	77
Total	519	163	31	264	62	23	255	101	40

1992A&AS...93..121N

TABLE 4a. *Detected sources.*

Source	Region	F_{12} (Jy)	F_{25} (Jy)	F_{60} (Jy)	rms (K)	T_{mb} (K)	v_o (km/s)	v_{exp} (km/s)	I_{co} (K km/s)	Ref	Ident.
00042 + 4248	IIIa	476.	324.	58.	0.103	0.37	−20.0	21.0	13.7	1	IRC+40004
00193 − 4033	IIIa	312.	152.	17.	0.025	0.06	−101.2	17.3	1.9		—
00213 + 3817	IIIa	327.	168.	24.	0.107	0.77	−15.0	12.7	11.7	1	R And
00245 − 0652	VII	116.	59.	11.	0.018	0.05	4.5	8.1	0.9		UY Cet
00247 + 6922	VII	306.	150.	29.	0.129	0.77	−28.6	17.8	17.3	3	AFGL67*
01037 + 1219	IIIa	1155.	967.	215.	0.129	0.92	8.5	21.6	28.2	8	IRC+10011
01085 + 3022	IIIa	165.	122.	19.	0.123	0.23	−25.0	15.0	5.7	2	IRC+30021
01159 + 7220	IIIa	342.	195.	27.	0.110	0.23	−26.0	19.0	6.0	3	S Cas
01556 + 4511	IIIa	499.	291.	42.	0.087	0.30	−2.2	9.4	3.7	3	BD44398
02143 + 4404	II	167.	72.	13.	0.087	0.43	−35.0	10.4	4.5	2	W And
02168 − 0312	II	4881.	2261.	301.	0.021	1.19	46.5	10.0	9.1	1	o Ceti
02270 − 2619	VII	254.	75.	16.	0.015	0.12	−2.6[a]	20.3	3.1	3	R For
02351 − 2711	IIIa	419.	255.	34.	0.020	0.10	−8.1	16.2	2.0	3	IRC-30023
02522 − 5005	II	729.	311.	53.	0.021	0.32	36.3	5.4	3.3	14	R Hor
03074 − 8732	IIIa	90.	87.	16.	0.012	0.10	7.3	10.3	1.2	15	—
03112 − 5730	II	101.	40.	7.	0.017	0.12	0.8	5.3	1.0	7	TW Hor
03186 + 7016	VII	146.	91.	23.	0.091	0.83	−16.4	8.3	9.0	1	AFGL482*
03229 + 4721	VII	535.	199.	40.	0.123	1.00	−16.2	14.5	25.0	8	IRC+50096
03287 − 1535	IIIa	53.	51.	13.	0.019	0.20	−4.6	8.2	1.6		—
03374 + 6229	VIa	121.	41.	17.	0.029	0.23	9.9	18.8	5.0	6	U Cam*
03448 + 4432	IIIa	130.	94.	22.	0.083	0.37	−25.0	16.0	11.3	3	AFGL5102
03507 + 1115	IIIa	4634.	2378.	332.	0.265	1.40	35.1	19.4	44.5	8	NML Tau
04307 + 6210	II	252.	92.	17.	0.097	0.80	−45.0	15.0	18.7	1	IRC+60144*
04395 + 3601	IV	471.	1107.	1035.	0.124	2.40	−22.8	19.6	61.4	8	AFGL 618
04459 + 6804	VII	95.	27.	6.	0.019	0.13	−15.0	10.0	2.1	6	ST Cam
04566 + 5606	VII	1640.	635.	134.	0.066	0.81	9.2	17.6	19.6	9	TX Cam*
04573 − 1452	VII	380.	116.	26.	0.020	0.24	22.7[a]	21.4	6.9	7	R Lep
05028 + 0106	VII	184.	52.	14.	0.046	0.21	5.2	11.8	3.7	6	W Ori
05052 − 8420	IIIa	282.	145.	20.	0.021	0.06	−3.7	14.5	1.3	15	NSV08135
05073 + 5248	IIIb	227.	274.	72.	0.093	0.57	3.0	18.0	19.7	1	IRC+50137*
05096 − 4834	II	197.	90.	15.	0.019	0.08	−0.1	11.8	0.8		S Pic
05098 − 6422	VII	129.	81.	16.	0.044	0.16	32.6	6.9	1.6		U Dor
05132 + 5331	II	459.	183.	22.	0.082	0.23	−3.3	11.1	2.6	1	R Aur
05151 + 6312	IIIa	328.	172.	25.	0.090	0.21	54.7	18.8	5.3	3	IRC+60154
05251 − 1244	V	38.	199.	103.	0.022	0.06	35.6	10.1	1.1		IC418
05411 + 6957	IIIa	801.	407.	52.	0.083	0.54	0.0	22.2	15.4	9	IRC+70066
05559 + 7430	IIIa	203.	106.	17.	0.076	0.20	7.6	15.1	3.7	5	V Cam
06012 + 0726	IIIa	320.	226.	56.	0.087	1.23	42.5	16.5	27.0	1	AFGL865
06192 + 4657	IIIa	41.	29.	6.	0.080	0.23	−22.7	7.7	2.3		—
06193 − 0349	IIIa	86.	61.	14.	0.018	0.08	−7.2	17.5	2.7		AFGL921
06230 − 0930	II	82.	35.	6.	0.023	0.08	25.1	14.4	1.4	2	AFGL935*
06297 + 4045	IIIa	103.	94.	21.	0.059	0.27	−17.9	17.6	6.3		IRC+40156
06300 + 6058	IIIa	296.	213.	45.	0.089	0.36	−23.1	19.7	10.0	1	IRC+60169
06331 + 3829	VII	232.	71.	18.	0.116	0.33	10.3	19.3	8.3	6	UU Aur
06582 + 1507	IIIb	39.	56.	17.	0.107	0.23	19.4	17.8	6.0		—
07027 − 7934	IV	23.	82.	42.	0.016	0.07	−27.2	14.5	1.3	16	—
07065 − 7256	II	203.	75.	14.	0.020	0.06	−3.2[a]	21.2	1.6	7	R Vol
07134 + 1005	V	25.	117.	50.	0.133	0.70	70.0	12.0	10.3	2	SAO96709
07152 − 3444	IIIa	205.	108.	14.	0.023	0.07	−16.4	18.1	1.2		AFGL1099
07203 − 3212	VII	40.	21.	4.	0.017	0.08	43.4	13.0	1.6		—
07209 − 2540	VII	9919.	6651.	1452.	0.019	0.06	24.2	30.8	2.4	3	VY CMa*
07245 + 4605	IIIa	122.	64.	11.	0.083	0.20	−0.7	8.6	2.2	10	Y Lyn
07373 − 4021	II	183.	68.	12.	0.037	0.14	11.7	24.4	5.1		CCS849
07454 − 7112	VII	613.	308.	65.	0.049	1.17	−38.7	13.6	23.3		—
07559 − 5859	VIa	102.	44.	54.	0.026	0.60	1.2	35.4	10.4		HR3126
07576 − 4054	VII	68.	39.	9.	0.021	0.11	3.6	7.0	1.4		—*
07582 − 1933	IIIa	82.	45.	9.	0.016	0.10	9.0	14.5	2.0	11	—
08171 − 2134	IIIa	120.	129.	39.	0.022	0.33	−9.0	16.3	7.9	3	AFGL5250
09076 + 3110	II	480.	209.	32.	0.068	0.77	7.5	7.0	7.3	1	RS Cnc*
09235 − 2347	IIIa	123.	89.	19.	0.044	0.13	13.3	18.0	3.4		IRC-20188
09425 + 3444	II	426.	176.	26.	0.057	0.18	1.5	6.5	2.2	12	R LMi
09425 − 6040	IIIb	27.	56.	21.	0.013	0.10	14.8	9.9	1.4		—*
09452 + 1330	VII	47530.	23070.	5652.	0.107	11.17	−26.2	15.7	275.7	1	IRC+10216
09521 − 7508	VII	345.	183.	35.	0.048	0.59	−3.6	12.8	10.6		AFGL4098
09533 − 4120	VII	89.	25.	6.	0.091	0.09	−17.5	8.6	1.3	7	X Vel
10131 + 3049	VII	3320.	1219.	274.	0.109	2.40	−1.9	17.5	77.5	8	CIT6
10323 − 4611	VII	537.	363.	69.	0.042	0.31	30.2	20.4	9.7		—
10329 − 3918	VIa	168.	45.	27.	0.030	0.51	24.4	21.2	11.1	7	U Ant
10350 − 1307	VII	206.	72.	17.	0.044	0.39	−31.9	7.9	4.7	7	U Hya
10491 − 2059	VII	1107.	459.	98.	0.050	1.40	−15.6	15.8	24.6	7	V Hya
10580 − 1803	IIIa	638.	307.	49.	0.019	0.26	10.7	10.3	5.0	3	R Crt
11296 − 4431	IIIa	43.	46.	9.	0.018	0.04	−0.9	17.2	1.3		—
11318 − 7256	VII	339.	114.	23.	0.015	0.17	−1.9	22.9	7.0		CCS1882
12379 − 4959	IIIa	85.	63.	12.	0.014	0.04	10.9	14.5	1.1		—
12380 + 5607	II	193.	91.	16.	0.065	0.33	16.8	8.8	2.9	5	Y Uma
12384 − 4536	IIIa	171.	153.	26.	0.048	0.14	−38.6	8.1	2.0		—
12394 − 4338	VII	159.	71.	14.	0.021	0.17	−31.9	16.1	5.1		NSV05868
12427 + 4542	VIa	276.	70.	17.	0.061	0.43	21.7	9.7	6.3	6	Y CVn
12447 + 0425	VII	230.	69.	14.	0.126	0.30	−0.8	19.9	8.3	1	RU Vir

TABLE 4a. *(continued)*

Source	Region	F_{12}	F_{25}	F_{60}	rms	T_{mb}	v_o	v_{exp}	I_{co}	Ref	Ident.
12540 − 6845	VII	264.	134.	32.	0.048	0.24	−34.7	28.8	9.9		—
13114 − 0232	IIIa	681.	340.	49.	0.021	0.36	−10.8	8.5	5.6	3	SW Vir
13482 − 6716	VII	110.	47.	11.	0.049	0.16	−39.7	16.5	3.9		—
14086 − 0730	IIIa	139.	102.	17.	0.015	0.06	−27.5	14.4	1.4		AFGL1686
14219 + 2555	IIIa	846.	419.	69.	0.078	0.70	1.1	10.8	10.0	1	RX Boo
14371 + 3245	IIIa	125.	70.	11.	0.067	0.20	5.7	8.1	2.0		RV Boo
14429 − 4539	IIIb	15.	33.	13.	0.011	0.06	−6.8	18.2	1.1		—
14591 − 4438	IIIa	304.	207.	29.	0.046	0.16	35.3	15.2	3.1		—
15082 − 4808	VII	793.	423.	96.	0.051	1.34	−3.3	20.4	42.4	14	AFGL4211
15094 − 6953	VII	201.	57.	15.	0.017	0.14	−1.9	8.5	2.1	7	X TrA
15148 − 4940	VII	188.	68.	14.	0.018	0.14	−42.7	26.9	6.9		CCS2232*
15226 − 3603	IIIa	166.	112.	16.	0.019	0.09	−60.0	15.0	2.0		AFGL1771
15332 − 6430	IIIa	67.	50.	11.	0.013	0.07	−27.9	17.5	1.7		—
15477 + 3943	VII	105.	32.	6.	0.049	0.10	−97.5	9.1	2.0	2	V CrB
16011 + 4722	IIIa	484.	241.	39.	0.071	0.46	−72.1	11.7	4.7	3	X Her
16029 − 3041	IIIb	142.	267.	83.	0.023	0.13	7.4[a]	17.1	3.1	14	AFGL1822
16105 − 4205	VIb	609.	806.	347.	0.020	0.81	−74.8[a]	17.7	19.1	4	—,*
16269 + 4159	II	438.	149.	23.	0.076	0.23	18.5	7.5	2.3	3	30g Her
16314 − 5611	IIIb	23.	32.	7.	0.014	0.04	−25.4	23.6	1.4		—
16418 + 5459	IIIa	131.	73.	12.	0.046	0.09	15.4	8.3	1.6		S Dra
17047 − 5650	IV	144.	257.	199.	0.017	0.21	−64.0	22.6	10.6	14	CPD-568032
17079 − 6554	VII	164.	63.	13.	0.049	0.23	−47.2	13.5	4.0		—
17102 − 1031	IIIa	171.	116.	20.	0.018	0.13	−31.0	11.7	2.0		IRC-10359*
17125 − 4814	IIIa	52.	58.	16.	0.016	0.06	−0.9	11.8	1.1		—
17267 − 1926	VIa	97.	26.	7.	0.022	0.11	28.3[a]	9.1	1.4	7	TW Oph*
17297 + 1747	IIIa	559.	408.	73.	0.161	1.00	−3.9	15.2	20.8	1	IRC+20326
17311 − 4924	V	18.	151.	58.	0.049	0.14	35.4	14.1	2.7	16	CD-4911554
17319 − 6234	IIIa	252.	296.	73.	0.052	0.21	−9.2	17.5	4.9		—
17389 − 5742	VII	115.	40.	10.	0.037	0.14	18.6	16.0	3.7		V Pav
17446 − 4048	IIIa	250.	127.	22.	0.050	0.21	−46.7	13.5	5.9		—
17446 − 7809	VII	422.	191.	40.	0.057	0.38	−0.8	15.9	8.5		—
17556 + 5813	VII	197.	66.	16.	0.101	0.20	−16.7	12.4	3.3	1	T Dra
18040 − 0941	VII	213.	85.	20.	0.031	0.19	30.4[a]	28.4	7.7	5	IRC-10396*
18240 + 2326	VII	731.	448.	88.	0.117	1.12	60.0	17.0	23.2	1	AFGL2155
18276 − 4717	VII	250.	85.	17.	0.055	0.30	12.2	22.2	7.6		—
18333 + 0533	IIIa	299.	317.	76.	0.260	0.67	30.0	20.0	16.7	1	AFGL2199
18349 + 1023	VII	719.	318.	66.	0.129	1.16	−30.2	17.0	29.4	9	IRC+10365
18397 + 1738	VII	534.	239.	60.	0.173	0.74	−1.1	15.0	14.4	8	IRC+20370
18401 + 2854	IIIa	94.	55.	7.	0.072	0.17	−30.2	12.3	2.7		FI Lyr
18467 − 4802	IIIb	285.	343.	72.	0.052	0.37	−45.9	13.6	7.1	14	—
18560 − 2954	VII	641.	331.	63.	0.019	0.37	3.1[a]	19.6	10.4	4	IRC-30398
19007 − 2247	VII	122.	55.	16.	0.052	0.19	39.0	15.9	3.1		SU Sgr
19007 − 3826	VII	153.	101.	26.	0.022	0.17	−50.8	22.5	6.4		AFGL5553
19017 − 0545	VIa	150.	38.	11.	0.023	0.12	64.3[a]	11.3	2.3	7	V Aql
19093 − 3256	IIIa	319.	210.	33.	0.055	0.16	37.7	14.2	3.3	14	V342 Sgr
19126 − 0708	II	1575.	669.	111.	0.050	0.96	−24.0	18.1	28.4	1	W Aql
19157 − 1706	IIIa	136.	89.	15.	0.018	0.06	−27.1	16.3	1.4		AFGL2361
19175 − 0807	VII	384.	193.	48.	0.021	0.16	27.9[a]	35.6	6.9	3	IRC-10502
19178 − 2620	IIIb	79.	97.	24.	0.017	0.11	3.6	18.0	2.9		AFGL2370
19247 − 1722	IIIa	90.	51.	9.	0.016	0.07	−37.0	11.7	1.2		IRC-20563
19474 − 0744	IIIa	461.	271.	47.	0.018	0.40	28.9	16.2	8.4	10	GY Aql*
19500 − 1709	V	28.	165.	73.	0.017	0.14	21.7	14.4	3.3	13	SAO163075
19550 − 0201	II	332.	151.	27.	0.021	0.21	24.4	11.7	3.1	3	RR Aql
19594 + 4047	IIIa	338.	260.	60.	0.093	0.57	30.0	22.1	19.3	3	AFGL2494
20038 − 2722	II	395.	152.	28.	0.049	0.13	−15.1	6.2	1.1	14	V1943 Sgr
20042 − 4241	IIIa	221.	158.	28.	0.015	0.14	−37.9	14.4	3.4		V2234 Sgr
20075 − 6005	IIIa	557.	273.	51.	0.043	0.17	−18.2	11.7	3.7	15	X Pav
20077 − 0625	IIIa	1255.	1061.	215.	0.024	0.60	−8.4[a]	16.9	14.3	1	IRC-10529
20120 − 4433	VII	38.	25.	10.	0.050	0.41	−29.2	12.5	7.4		RZ Sgr
20135 − 7152	IIIa	119.	93.	16.	0.013	0.03	−2.8	17.3	1.0	15	NSV12961
20141 − 2128	VII	73.	21.	4.	0.048	0.05	−19.9	9.1	0.6	7	RT Cap
20234 − 1357	IIIa	47.	45.	11.	0.026	0.08	−20.6[a]	10.7	1.4	17	OH30.7-27.1
20248 + 7505	IIIa	132.	90.	13.	0.067	0.23	−25.0	10.0	3.0		UU Dra
20248 − 2825	II	494.	192.	32.	0.021	0.11	22.6	8.1	1.4		T Mic
20440 − 0105	IIIa	211.	117.	17.	0.044	0.10	9.0	10.8	2.3	5	AFGL2646
20484 − 7202	IIIa	179.	110.	14.	0.018	0.07	−41.5	14.4	1.3		—
20541 − 6549	IIIa	180.	89.	15.	0.013	0.04	−4.5	19.0	1.4	15	—
21032 − 0024	VII	308.	116.	22.	0.022	0.31	1.0	16.1	7.9	7	RV Aqr
21044 − 1637	IIIa	229.	113.	17.	0.018	0.06	−5.5	9.1	0.8		RS Cap
21069 − 3843	IIIa	171.	116.	16.	0.036	0.11	−24.0	11.6	1.9		AFGL5592
21197 − 6956	VII	73.	27.	7.	0.024	0.12	5.4[a]	14.0	2.3	7	Y Pav
21320 + 3850	VII	257.	94.	20.	0.103	0.60	−5.0	13.0	13.0	1	IRC+40485
21358 + 7823	VII	383.	133.	29.	0.125	0.50	−15.9	31.3	20.0	3	S Cep*
21399 + 3516	VIa	78.	21.	9.	0.035	0.26	27.0	11.4	4.7	6	V460 Cyg
21412 + 3747	VII	103.	32.	11.	0.027	0.23	16.8	14.7	4.8	6	RV Cyg
21439 − 0226	IIIa	637.	320.	47.	0.052	0.30	−34.8	11.3	5.0	3	EP Aqr*
21554 + 6204	IIIb	68.	152.	53.	0.093	0.32	−17.8	18.2	7.7	3	—
22190 − 0751	IIIa	81.	44.	7.	0.021	0.07	15.3	8.2	0.7		IRC-10580
22196 − 4612	IIIa	908.	436.	77.	0.050	0.33	−13.2	19.4	6.9	14	π^1 Gru
23166 + 1655	IIIa	707.	775.	249.	0.123	1.60	−31.0	15.1	31.0	8	AFGL3068
23213 − 4521	IIIa	128.	96.	17.	0.039	0.11	−5.2	18.9	2.4	15	AFGL4296
23320 + 4316	VII	960.	468.	111.	0.093	1.40	−17.0	14.4	35.7	8	IRC+40540
23438 + 0312	VIa	163.	40.	12.	0.044	0.29	12.9	11.8	4.7	6	TX Psc
23558 + 5106	II	1340.	555.	102.	0.049	0.81	24.7	14.3	14.4	9	R Cas

1992A&AS...93..121N

TABLE 4b. *Tentative detections.*

Source	Region	F_{12} (Jy)	F_{25} (Jy)	F_{60} (Jy)	rms (K)	Ref[b]	Identification
03488 + 3943	VII	141.	39.	8.	0.134		IRC+40070
04179 + 5951	VII	57.	27.	7.	0.082		AFGL5118*
04287 + 1801	V	10.	106.	373.	0.123		L1551(B)*
04296 + 3429	V	13.	46.	15.	0.090	19	—*
04328 + 2824	II	55.	22.	4.	0.061		IRC+30090
04396 + 0647	IIIa	49.	30.	6.	0.163		AFGL619
05104 + 2055	VII	90.	32.	8.	0.065	11	—
05440 + 4311	IIIa	47.	27.	4.	0.061		IRC+40140
06363 + 5954	II	110.	47.	6.	0.076		U Lyn
12544 + 6615	VII	108.	31.	8.	0.068	6	RY Dra
13001 + 0527	IIIa	462.	226.	39.	0.071	4	RT Vir
14353 − 4809	IIIb	21.	28.	6.	0.014		—
14550 − 1214	II	91.	43.	7.	0.015		AFGL1743
15060 + 0947	IIIa	35.	27.	4.	0.081		—
15193 + 3132	IIIa	201.	126.	19.	0.113	20	S CrB
15223 − 0203	IIIa	101.	66.	11.	0.014		AFGL1769
15483 + 1517	II	191.	71.	11.	0.093		R Ser
16574 − 1032	IIIa	90.	52.	7.	0.014		IRC-10355
17119 + 0859	IIIa	460.	317.	41.	0.000		AFGL1940
17123 + 1107	II	62.	27.	4.	0.191		V438 Oph
17265 − 0725	IIIa	142.	81.	13.	0.016		AFGL1970*
17329 + 5359	VII	35.	21.	4.	0.263		IRC+50267
17534 + 2603	VII	98.	55.	13.	0.096	13	V441 Her (F)
18112 + 1227	IIIa	37.	24.	4.	0.097		V454 Oph
19354 + 5005	VII	105.	52.	12.	0.090	2	R Cyg
19375 + 4322	IIIa	26.	23.	4.	0.104		—
19585 + 5200	II	50.	20.	3.	0.098		AFGL2490
20079 − 0146	II	60.	29.	5.	0.024		IRC-10529*
20443 + 0215	II	70.	25.	3.	0.130		V Aqr
20444 + 0540	IIIa	34.	29.	6.	0.102		EIC837*
21306 + 4422	V	11.	47.	24.	0.106	18	IC5117
21453 + 5959	IIIa	26.	21.	4.	0.179		—*
22035 + 3506	IIIa	265.	146.	23.	0.133	4	SV Peg
22223 + 4327	V	2.	37.	23.	0.090		—
22233 + 3013	IIIa	124.	72.	11.	0.061		RV Peg
22476 + 4047	VII	99.	33.	8.	0.066		RX Lac
22525 − 2952	II	247.	110.	18.	0.013	14	V PsA
23279 + 5336	VII	67.	33.	7.	0.123	11	—
23541 + 7031	VIb	91.	92.	55.	0.062		AFGL3181*
23554 + 5612	VII	51.	28.	9.	0.078		IRC+60431

TABLE 4c. *Non detections*

Source	Region	F_{12} (Jy)	F_{25} (Jy)	F_{60} (Jy)	rms (K)	Ref[b]	Identification
00001 + 4826	IIIa	49.	24.	4.	0.148		IW Cas
00007 + 5524	IIIa	98.	47.	7.	0.066		Y Cas
00102 + 7214	V	15.	72.	64.	0.090		NGC40
00127 + 5437	IIIa	56.	40.	5.	0.091		—
00128 − 3219	II	104.	38.	7.	0.023		S Scl
00192 − 2020	VII	198.	56.	14.	0.017		T Cet
00428 + 6854	IIIa	71.	51.	10.	0.084		IRC+70012*
00506 + 5224	IIIa	41.	36.	5.	0.211		IRC+50018
01005 + 7910	V	4.	24.	10.	0.079		—
01010 + 7434	VII	64.	24.	5.	0.153		IRC+70016
01217 + 2341	IIIa	40.	20.	3.	0.123		IRC+20023
01438 + 1850	IIIa	77.	40.	7.	0.110		SV Psc
01527 + 1656	IIIa	35.	20.	3.	0.060		AFGL4013
01597 + 5459	II	71.	29.	4.	0.164		XX Per*
02152 + 2822	IIIa	121.	112.	29.	0.083	3	—
02302 + 4525	IIIa	134.	81.	11.	0.073		SAO38115
02339 + 3402	II	59.	20.	3.	0.058		R Tri
02384 + 3418	IIIa	43.	21.	3.	0.173		W Tri
02407 + 3602	IIIa	61.	49.	8.	0.121		TV Per
02441 + 6922	IV	13.	22.	16.	0.115		AFGL5081*
03082 + 1436	II	71.	26.	5.	0.114		U Ari
03157 + 3258	IIIa	46.	26.	5.	0.066		—
03170 + 3150	IIIa	64.	41.	7.	0.097		UZ Per*
03206 + 6521	IIIb	96.	134.	37.	0.093	17	OH138.0-7.3*
03318 − 1619	II	158.	62.	10.	0.020		RT Eri
03364 − 5533	II	69.	29.	4.	0.044		SAO233190
03415 + 8010	VII	114.	55.	11.	0.087		SS Cep
03449 + 6522	VIa	95.	26.	14.	0.053		AFGL520*
03482 − 5213	II	59.	28.	4.	0.045		SAO233291
03489 − 0131	II	80.	38.	6.	0.042		SU Eri
03490 + 4455	IIIa	42.	24.	4.	0.092		IRC+40071
03513 + 1801	IIIa	33.	24.	8.	0.165		—
03557 + 4404	IIIa	36.	30.	8.	0.080		AFGL5110
04020 − 1551	IIIa	326.	184.	23.	0.019	3	V Eri
04094 − 2515	II	97.	42.	6.	0.011		W Eri
04137 + 3114	IIIa	58.	30.	5.	0.180		IRC+30080
04140 − 8158	II	339.	160.	24.	0.018		U Men
04155 + 2812	IV	33.	100.	72.	0.070		AFGL5117*
04166 + 4056	IIIa	196.	113.	16.	0.090		IR Per*

TABLE 4c. *(continued)*

Source	Region	F_{12}	F_{25}	F_{60}	rms	Ref[b]	Identification
04188 + 2819	IIIb	18.	26.	15.	0.100		RY Tau*
04265 + 5718	VII	59.	35.	8.	0.096		RV Cam
04269 + 3510	VIb	362.	340.	3119.	0.117		AFGL585*
04280 + 2722	IIIa	42.	22.	4.	0.150		IRC+30087*
04292 + 3100	IIIa	41.	24.	3.	0.070		IRC+30088*
04382 − 1417	IIIa	105.	54.	8.	0.020		BX Eri
04386 + 5722	IIIb	18.	23.	4.	0.136		—
04387 − 3819	II	158.	67.	9.	0.015		R Cae
04404 − 7427	IIIa	65.	49.	7.	0.048		SY Men
04575 + 1251	IIIa	133.	122.	19.	0.117		AFGL5134*
05027 − 2158	IIIa	157.	82.	12.	0.022		T Lep
05069 − 3434	VII	99.	38.	8.	0.022		SAO195594
05089 + 0459	IV	7.	22.	11.	0.099		—
05090 − 1154	II	280.	124.	19.	0.023		RX Lep
05136 + 4712	VII	53.	24.	5.	0.088	11	—
05223 + 4704	VII	62.	25.	5.	0.092		—*
05265 − 0443	II	151.	64.	12.	0.020		S Ori
05280 − 6910	V	4.	24.	12.	0.019		56-SC132
05351 − 0147	IIIa	96.	49.	6.	0.022		X Ori
05361 + 4644	IIIa	186.	191.	66.	0.095		IRC+50149
05404 − 2343	IIIa	75.	37.	6.	0.036		RT Lep
05411 − 8625	II	91.	43.	7.	0.028		R Oct
05450 − 3142	II	48.	21.	3.	0.018		S Col
05513 − 1024	IV	18.	26.	28.	0.037		—*
05524 + 0723	II	4682.	1738.	299.	0.132	1	α Ori
05534 + 4530	II	132.	63.	8.	0.079		TW Aur
05535 + 4822	IIIa	41.	26.	4.	0.212		IRC+50154*
05543 + 5002	VII	31.	22.	4.	0.056		—*
05559 + 3825	IIIa	118.	70.	9.	0.103	21	IRC+40149*
05592 − 0221	IIIa	156.	88.	13.	0.035		V352 Ori
06003 + 4747	IIIa	35.	27.	5.	0.078		—*
06027 − 1628	VII	143.	72.	14.	0.049		SAO151093 (A0)
06036 − 2411	IIIa	258.	141.	17.	0.039		S Lep
06038 − 0541	VII	48.	25.	5.	0.036		IRC-10109*
06053 − 0622	V	470.	4095.	13070.	0.099		Outflow*
06084 − 0611	V	27.	602.	3607.	0.026		Outflow*
06139 + 3313	IIIa	107.	53.	9.	0.054		VW Aur*
06176 − 1036	IIIa	422.	455.	173.	0.026		AFGL915 (Be)
06250 + 6134	IIIa	39.	28.	5.	0.083		V Lyn
06255 − 4928	IIIa	66.	43.	6.	0.018		—
06259 − 1301	IIIa	146.	143.	25.	0.026		SAO151134(B0p)
06278 + 2729	II	161.	76.	10.	0.103		DW Gem
06291 + 4319	II	107.	51.	9.	0.196	2	AFGL954
06319 − 0501	VIb	51.	65.	26.	0.044		AFGL5201
06403 − 1424	VII	39.	22.	4.	0.018		DY CMa
06434 − 3628	VII	48.	25.	5.	0.021		CH Pup
06496 − 1858	IIIa	72.	42.	7.	0.017		IRC-20110
07034 − 3551	IIIa	253.	136.	17.	0.018		SAO197549
07051 + 6601	IIIa	53.	32.	5.	0.097		IRC+70074
07113 − 2747	IIIb	18.	27.	8.	0.023		—
07120 − 4433	II	2415.	845.	94.	0.019		L2 Pup
07150 + 3808	II	107.	47.	8.	0.095		IRC+40172
07299 + 0825	II	103.	41.	6.	0.089		S CMi
07308 + 3037	IIIa	226.	122.	14.	0.098		AFGL1141
07331 + 0021	V	15.	68.	18.	0.084		AI CMi
07430 + 1115	V	8.	30.	11.	0.131		—
07434 − 3750	VII	605.	257.	49.	0.046		SAO198398 (K5)
07585 − 1242	IIIa	91.	53.	7.	0.044		U Pup
08003 + 3629	IIIa	52.	29.	5.	0.093		SV Lyn
08063 + 6522	II	47.	22.	4.	0.080		RZ UMa
08138 + 1152	II	293.	109.	18.	0.107		R Cnc
08189 + 0507	IIIa	76.	38.	6.	0.142		FZ Hya
08196 + 1509	IIIa	44.	22.	3.	0.127		Z Cnc
08272 − 0609	II	106.	41.	6.	0.017		RT Hya
08349 − 5945	II	122.	49.	7.	0.049		KK Car
08357 − 1013	IIIa	63.	59.	11.	0.053		—
08372 − 0924	IIIa	77.	40.	6.	0.013		RV Hya
08375 − 1707	IIIa	192.	93.	15.	0.041		AK Hya
08391 + 0222	IIIa	56.	41.	7.	0.093		AFGL1283
08437 + 0149	IIIa	102.	50.	8.	0.098		EY Hya
08440 + 1803	V	2.	42.	89.	0.059		PK208+33.1
08525 + 1725	VII	90.	26.	7.	0.078	6	X Cnc
08555 + 1102	II	73.	29.	4.	0.263		RT Cnc
09057 + 1325	IIIa	90.	45.	8.	0.190		AFGL1321
09069 + 2527	IIIa	64.	33.	6.	0.063		W Cnc
09072 − 5933	IIIa	62.	50.	8.	0.023		—*
09256 − 6324	IIIa	101.	96.	34.	0.048		IW Car
09309 − 6234	II	475.	170.	24.	0.049		R Car
09331 − 1428	II	97.	38.	5.	0.016		X Hya
09373 − 5951	V	4.	27.	19.	0.020		PK281-5.1
09480 − 4147	IIIa	149.	89.	17.	0.018		SU Vel*
10189 − 3432	IIIa	73.	43.	6.	0.016		V Ant

1992A&AS...93..121N

TABLE 4c. *(continued)*

Source	Region	F_{12}	F_{25}	F_{60}	rms	Ref[b]	Identification
10383 − 7741	IIIa	53.	27.	5.	0.018		NSV04933*
10411 + 6902	IIIa	94.	55.	7.	0.058		R UMa
10521 + 7208	VII	36.	20.	4.	0.102		IRC+70102
11011 − 6651	IIIa	43.	21.	4.	0.014		KV Car
11072 − 7727	V	12.	83.	233.	0.035		Cham I*
11125 + 7524	IIIa	91.	50.	7.	0.125		IRC+80023
11252 + 1525	IIIa	48.	31.	4.	0.078		AF Leo
11312 − 6955	V	66.	243.	165.	0.021		SAO252457 (B9)*
11445 + 4344	IIIa	75.	53.	7.	0.063		AFGL1511
11466 − 4128	II	120.	46.	7.	0.024		X Cen*
11494 − 5620	IIIa	45.	30.	4.	0.025		—
11525 − 5057	IIIa	95.	72.	12.	0.050		—
11538 + 5808	II	65.	26.	4.	0.107		Z UMa
11575 − 7754	VIb	24.	23.	15.	0.025		SAO256895
12175 − 5338	V	1.	21.	7.	0.025		SAO239853
12226 + 0102	VII	92.	29.	6.	0.092		SS Vir
12277 + 0441	II	249.	102.	19.	0.110	5	BK Vir
12344 + 2720	IIIa	76.	38.	5.	0.062		IRC+30241
12387 − 3717	IIIa	97.	61.	8.	0.019		—
12584 − 4837	IIIb	36.	49.	13.	0.016		CD-487859
13203 − 5536	IIIa	134.	107.	20.	0.037		—*
13266 − 5551	V	1.	36.	35.	0.025		CPD-555558*
13269 − 2301	II	1591.	585.	90.	0.040	3	R Hya
13303 − 0656	II	135.	55.	8.	0.024		S Vir
13368 − 4941	IIIa	222.	115.	17.	0.019		V744 Cen
13468 + 3947	II	103.	41.	6.	0.054		R CVn
13479 − 5436	IIIa	92.	77.	12.	0.016		—
13582 + 3806	IIIa	43.	27.	5.	0.066		SAO63879
14003 − 7633	II	734.	340.	53.	0.019		θ Aps
14020 − 3515	II	241.	94.	13.	0.018		AQ Cen
14086 − 6907	IIIa	94.	83.	13.	0.046		—*
14162 + 6701	II	62.	25.	3.	0.130		U UMi
14180 − 7107	IIIa	44.	28.	4.	0.025		—
14247 + 0454	IIIa	109.	65.	12.	0.080		RS Vir
14249 − 5310	IV	12.	29.	23.	0.020		—*
14280 − 2952	II	154.	63.	10.	0.049		Y Cen
14390 + 3147	IIIa	61.	30.	6.	0.089		RW Boo
14453 − 4920	IIIa	56.	39.	7.	0.019		—
15134 − 4527	V	3.	34.	49.	0.020		PK327+10.1*
15214 − 2244	II	189.	66.	12.	0.018		RS Lib
15255 + 1944	IIIa	235.	150.	18.	0.061	20	WX Ser
15262 + 0400	IIIa	46.	31.	5.	0.114		IRC+00266
15314 + 7847	II	146.	59.	7.	0.081		S UMi
15318 − 7144	V	7.	105.	62.	0.021		PK315-13.1*
15341 + 1515	IIIa	188.	91.	16.	0.088		τ^4 Ser
15356 − 6722	IIIa	65.	64.	11.	0.016		—
15410 − 0133	II	119.	47.	7.	0.019		BG Ser
15422 − 4414	IIIb	29.	44.	12.	0.020		—
15492 + 4837	IIIa	199.	97.	17.	0.073	20	ST Her
15513 − 6600	V	2.	48.	43.	0.021		He2-138
15566 + 3609	IIIa	53.	28.	3.	0.069		RS CrB
15568 − 4513	II	159.	67.	8.	0.049		—
15589 − 2850	VII	76.	42.	8.	0.021		SAO184042
16005 − 4126	IIIb	30.	39.	8.	0.022		—*
16074 − 3639	IIIa	50.	47.	10.	0.021		NSV07495
16081 + 2511	II	173.	78.	11.	0.076		RU Her
16114 − 5946	V	2.	23.	7.	0.021		PK326-6.1
16235 + 1900	II	500.	180.	27.	0.060		U Her
16245 − 3859	V	4.	25.	31.	0.018		—*
16260 + 3454	IIIa	62.	50.	10.	0.064		IRC+30292
16306 + 7223	II	106.	45.	7.	0.092		R UMi
16342 − 3814	V	16.	200.	290.	0.020		High vel. OH maser
16416 − 2758	V	9.	37.	29.	0.019		PK352+11.2
16423 + 2353	V	2.	26.	35.	0.140		PK43+37.1
16438 − 1133	II	139.	58.	9.	0.025		V446 Oph
16456 − 3542	V	5.	30.	11.	0.026		PK347+ 5.1*
16473 + 5753	II	63.	24.	4.	0.110		AH Dra
16494 − 1252	IIIa	84.	44.	7.	0.018		IRC-10348
16534 − 3030	II	189.	70.	12.	0.021		RR Sco
16559 − 2957	IV	9.	32.	16.	0.028		—*
16589 − 3315	IIIa	60.	59.	9.	0.021		—*
17001 − 2029	VII	46.	31.	7.	0.018		IRC-20341
17020 − 5254	IIIa	79.	58.	8.	0.046		—
17026 − 4932	IIIb	20.	27.	5.	0.022		—
17028 − 1004	IV	51.	110.	123.	0.017	18	M2-9*
17081 + 6422	II	60.	26.	5.	0.083		TV Dra
17122 − 2707	IIIa	48.	54.	17.	0.017		—*
17123 + 1426	VII	1515.	428.	83.	0.073		α Her
17132 − 5003	IIIa	40.	45.	8.	0.020		—
17139 + 0446	II	54.	22.	3.	0.161		UY Oph
17174 − 4641	IIIa	83.	59.	9.	0.048		—
17180 − 2708	V	2.	20.	32.	0.024		519-PN13 Pl*
17189 − 6501	IIIb	30.	41.	9.	0.046		—

TABLE 4c. *(continued)*

Source	Region	F_{12}	F_{25}	F_{60}	rms	Ref[b]	Identification
17215 − 7114	IIIa	108.	106.	30.	0.051		—
17230 + 0113	IIIa	25.	22.	4.	0.106		AFGL6826S
17262 − 2343	V	9.	66.	109.	0.025		PK2+5.1*
17294 − 4326	IIIa	94.	70.	10.	0.017		—
17313 − 1531	IIIa	63.	56.	9.	0.019		—
17331 − 1618	IIIb	95.	114.	22.	0.018		AFGL5359
17436 + 5003	V	6.	184.	151.	0.110	13	HD161796
17484 − 0800	IIIa	190.	123.	16.	0.046		IRC-10381*
17531 − 0940	IIIb	18.	35.	12.	0.020		—*
17539 + 1037	IIIa	48.	28.	4.	0.200		IRC+10340
17541 + 1110	II	59.	27.	4.	0.338		RT Oph
17567 − 3849	V	3.	30.	20.	0.025		PK352-07.1
17570 − 3713	IIIa	118.	60.	9.	0.018		EK Cra
17579 + 2335	IIIa	63.	36.	5.	0.079		WY Her
17584 + 6638	V	8.	114.	133.	0.077		PK96+29.1
17599 − 3653	IIIa	114.	62.	11.	0.051		AFGL5430
18006 − 3213	IIIa	28.	31.	12.	0.022		—*
18069 + 0911	IIIa	69.	62.	11.	0.102		—
18076 + 3445	IIIa	32.	27.	5.	0.084		—
18081 − 0338	IV	26.	69.	23.	0.018		—*
18092 − 0437	IIIa	142.	110.	22.	0.020		AFGL2088*
18095 + 2704	V	45.	126.	28.	0.113		—
18096 + 0650	V	24.	169.	95.	0.092		PK34+11.1
18125 + 3010	IIIa	52.	27.	5.	0.580		IRC+30330
18129 − 3053	V	18.	86.	24.	0.012		PK 1-6.2
18157 + 1757	VII	64.	21.	6.	0.079		IQ Her
18186 + 3143	IIIa	66.	36.	6.	0.079		TU Lyr
18213 + 0335	IIIa	99.	51.	7.	0.107		IRC+00349
18222 + 3933	II	47.	21.	3.	0.092		TW Lyr
18237 − 2408	IIIb	18.	24.	6.	0.027		—*
18243 + 0352	IIIa	79.	39.	4.	0.136		V988 Oph
18276 + 8236	IIIa	45.	30.	5.	0.078		AFGL2171
18280 − 5639	II	150.	65.	10.	0.053		SS Tel
18281 + 2149	IIIb	42.	65.	21.	0.061		AC Her
18298 − 2111	IIIb	43.	96.	40.	0.051		—*
18359 + 0847	II	409.	146.	22.	0.119		X Oph
18379 − 1707	V	2.	24.	7.	0.022		—*
18409 + 1220	IIIa	86.	51.	7.	0.091		IRC+10373*
18430 − 1430	V	2.	27.	17.	0.020		M1-61*
18436 + 4334	IIIa	65.	51.	10.	0.073		RW Lyr
18491 − 3648	IIIb	12.	21.	8.	0.021		—
18512 + 2029	IIIa	36.	34.	5.	0.095		—
18520 − 1635	IIIa	97.	53.	7.	0.019		UX Sgr
18540 + 3005	IIIa	78.	41.	5.	0.144		IRC+30347
19016 − 2330	V	13.	58.	28.	0.026		—
19029 + 2017	VII	76.	36.	8.	0.169		AFGL2318*
19031 + 2702	IIIa	48.	24.	4.	0.100		IRC+30355
19032 − 4602	IIIa	100.	65.	10.	0.040		RX Tel
19042 − 4858	IIIa	206.	126.	18.	0.020		U Tel
19098 + 6601	IIIa	42.	25.	4.	0.284		SZ Dra
19143 − 5032	IIIa	111.	65.	10.	0.021		V Tel
19158 + 0141	V	5.	30.	40.	0.114		V605 Aql
19161 + 2343	IIIb	112.	137.	31.	0.098	4	AFGL2362
19204 + 0124	IV	14.	35.	13.	0.120		NSV11959-*
19231 + 3555	IIIa	112.	90.	13.	0.091		IRC+40346
19231 − 2717	VIb	26.	33.	15.	0.016		—
19240 + 3615	IIIa	97.	81.	11.	0.123		—
19243 + 7135	II	49.	22.	3.	0.067		YZ Dra
19287 + 4602	II	78.	35.	4.	0.084		AF Cyg
19288 + 2923	IIIb	41.	57.	14.	0.087		—*
19296 + 4331	IIIa	104.	59.	10.	0.081		UV Cyg
19324 + 3033	VII	38.	20.	4.	0.113		HR Cyg
19327 + 3024	IV	89.	235.	161.	0.100		PK64+ 5.1
19328 + 0035	IIIa	43.	22.	4.	0.068		V607Aql
19361 − 1658	IIIa	98.	76.	10.	0.018		AFGL2425
19374 + 0550	IIIa	155.	115.	15.	0.097		EIC786
19422 + 3506	IIIa	203.	172.	28.	0.095		AFGL2445
19434 + 5024	V	5.	39.	46.	0.116		PK83+12.1
19510 − 5919	II	502.	204.	29.	0.048		S Pav
19528 − 2919	II	142.	54.	8.	0.052		RR Sgr
20000 + 4954	IIIa	81.	67.	11.	0.089		Z Cyg
20047 + 1248	IIIa	65.	33.	5.	0.209		SY Aql
20113 + 4917	IIIa	100.	54.	8.	0.087		AC Cyg
20181 + 2234	IIIb	26.	33.	7.	0.133		—*
20381 + 5001	IIIa	33.	26.	4.	0.105		—
20406 + 2953	V	13.	68.	49.	0.067		—*
20431 + 1754	IIIa	142.	78.	11.	0.133		U Del
20532 + 5554	IIIa	59.	44.	10.	0.130	22	—*
21014 − 1133	V	6.	57.	91.	0.015		PK37-34.1
21027 + 3704	II	92.	37.	6.	0.102		GR Cyg
21088 + 6817	II	754.	267.	41.	0.120	5	T Cep
21120 + 0736	IIIa	34.	26.	3.	0.104		—
21208 + 7737	IIIa	71.	34.	6.	0.090		GH Cep
21245 + 6221	IIIa	78.	58.	10.	0.160		SW Cep*

1992A&AS...93..121N

TABLE 4c. *(continued)*

Source	Region	F_{12}	F_{25}	F_{60}	rms	Ref[b]	Identification
21270 + 7135	IIIa	106.	54.	8.	0.097		IRC+70171*
21368 − 3812	VII	55.	33.	7.	0.020		—
21414 + 7609	IIIa	48.	24.	4.	0.073		IRC+80049*
21426 + 1228	II	60.	27.	4.	0.092		TU Peg
21440 + 7324	VII	138.	42.	9.	0.137	2	IRC+70177*
21456 + 6422	IIIa	175.	108.	16.	0.070	20	RT Cep
21543 − 1421	IIIa	75.	47.	8.	0.049		SAO164760
22142 − 8454	IIIa	143.	72.	11.	0.021		SAO258927
22230 − 4841	II	129.	58.	9.	0.017		S Gru
22231 − 4529	IIIa	115.	65.	8.	0.016		—
22359 − 1417	IIIa	39.	20.	3.	0.024		AB Aqr
22516 + 0838	IIIa	113.	64.	11.	0.104		IRC+10523
22518 + 6600	VII	80.	34.	8.	0.208	5	AFGL2985
22540 − 5740	II	125.	56.	9.	0.019		SAO247653
23013 + 3735	IIIa	109.	61.	8.	0.129		SAO72968
23041 + 1016	II	183.	73.	11.	0.097		R Peg
23063 − 3024	II	112.	47.	6.	0.048		Y Scl
23134 − 7031	II	108.	38.	6.	0.020		SAO258124
23173 + 2600	II	218.	94.	13.	0.100		W Peg
23212 + 3927	II	104.	46.	7.	0.147		BU And
23234 + 4215	V	4.	35.	37.	0.128		PK106-17.1
23268 + 6854	VIb	27.	36.	42.	0.186	23	—
23365 + 5159	IIIa	128.	81.	12.	0.113		SV Cas
23412 − 1533	II	1577.	543.	66.	0.018		R Aqr
23425 + 4338	IIIa	72.	54.	9.	0.072		EY And
23528 + 4821	II	123.	56.	9.	0.079		RS And
23564 − 5651	IIIa	80.	40.	5.	0.045		S Phe
23575 + 2536	II	54.	23.	3.	0.079		Z Peg

1. Knapp & Morris (1985), 2. Zuckerman et al. (1986), 3. Zuckerman & Dyck (1986a), 4. Zuckerman & Dyck (1986b), 5. Zuckerman & Dyck (1989), 6. Olofsson et al. (1987), 7. Olofsson et al. (1988), 8. Sopka et al. (1989), 9. Lindqvist et al. (1988), 10. Wannier & Sahai (1986), 11. Nguyen-Q-Rieu et al. (1987), 12. Knapp et al. (1982), 13. Likkel et al. (1987), 14. Knapp et al. (1989), 15. Deguchi et al. (1990), 16. Loup et al. (1990), 17. Heske et al. (1990), 18. Huggins & Healy (1989), 19. Woodsworth et al. (1990), 20. Margulis et al. (1990), 21. Knapp (1986), 22. Leahy et al. (1987), 23. Arquilla et al. (1986)

An asterisk (*) after the name of the object signifies that there is an interstellar line in the CO spectrum. In a few cases the spectral type of the object is given within parenthesis.
a. The centre velocity is uncertain up to ±10 kms^{-1} (see text).
b. Previous CO detections. For sources previously detected in CO (1–0) emission and not detected by us, the CO (1–0) line was usually too weak to be seen with our sensitivity limit, and in a few cases it may only have been a tentative detection. Sources detected in the CO (2–1) line are also listed as previous detections. The CO (2–1) line can be brighter than the (1–0) line because of optical depth and beam filling effects, and the (1–0) line may be too weak to be detected.

TABLE 5. *CO parameters as function of IRAS regions.*

Region	v_{exp}	Δv_{exp}	K_{60}	A_{60}	r_{60}	n
II	11.4	5.4	0.64±0.19	−0.48±0.28	0.63	19
IIIa	14.5	4.0	0.87±0.06	−0.76±0.09	0.88	67
IIIb	17.2	3.7	0.68±0.20	−0.51±0.30	0.79	9
IV	18.9					
V	12.7	2.0				
VIa	16.1	8.9	1.03±0.18	−0.67±0.21	0.92	8
VIb	17.7					
VII	16.6	6.6	0.91±0.07	−0.50±0.10	0.87	50

r_{60} is the correlation coefficient to the fit $\log(I_{CO}) = K_{60} \cdot \log(F_{60}) + A_{60}$ and n is the number of sources included in the fit.

TABLE 6. *Objects with Cold Envelopes.*

Source	Region	Det[a]	Ref[b]	Identification	Sp.type	Ref[c]
00102 + 7214	V	N		PK120+9.1, NGC40		1
01005 + 7910	V	N		—		
02441 + 6922	IV	N*		AFGL5081		
03206 + 6521	IIIb	N*	16	OH 138.0-7.3		
03374 + 6229	VIa	D	17	U Cam	N5	15
03449 + 6522	VIa	N*		SAO12916	M0	
04155 + 2812	IV	N*		V892 Tau (Herbig Ae/Be)	Ae/Be	13
04188 + 2819	IIIb	N*		RY Tau (T Tauri star)	F8	
04269 + 3510	VIb	N*		AFGL585 (Young Obj.)		
04287 + 1801	V	?*		L1551(B) (Young Obj.)		8
04296 + 3429	V	?*	18	—	F-G	3
04386 + 5722	IIIb	N		—		
04395 + 3601	IV	D	19	AFGL 618		6
05073 + 5248	IIIb	D*	20	IRC+50137		
05089 + 0459	IV	N		—		
05251 − 1244	V	D		PK215-24.1, IC418		1,2
05280 − 6910	V	N		NGC1984 (in LMC)		
05513 − 1024	IV	N*		—		
06053 − 0622	V	N*		Outflow (Young Obj.,See Sect. 5.4)		
06084 − 0611	V	N*		Outflow (Young Obj.,See Sect. 5.4)		
06319 − 0501	VIb	N		AFGL5201		
06582 + 1507	IIIb	D		—		
07027 − 7934	IV	D	21	—	WC11	11
07113 − 2747	IIIb	N		—		
07134 + 1005	V	D	22	SAO96709	F5	2,3
07331 + 0021	V	N		AI CMi	G5	2
07430 + 1115	V	N		—		
07559 − 5859	VIa	D		HR3126	MIII	30
08440 + 1803	V	N		PK208+33.1		
09373 − 5951	V	N		PK281-5.1		
09425 − 6040	IIIb	D		—		
10329 − 3918	VIa	D	23	U Ant	N	
11072 − 7727	V	N*		Cham I (Young Obj.)		7
11312 − 6955	V	N*		SAO251457 (Herbig Ae/Be)	B9	12
11575 − 7754	VIb	N		SAO256895 (Herbig Ae/Be)	Ae/Be	12
12175 − 5338	V	N		SAO239853	F2	2
12427 + 4542	VIa	D	17	Y CVn	N3	15
12584 − 4837	IIIb	N		CD − 487859		
13266 − 5551	V	N*		CPD − 555558		
14249 − 5310	IV	N*		—		
14353 − 4809	IIIb	?		—		
14429 − 4539	IIIb	D		—	G0	13
15134 − 4527	V	N*		PK327+10.1		
15318 − 7144	V	N*		PK315-13.1		1,2
15422 − 4414	IIIb	N		—		
15513 − 6600	V	N		He2-138		
16005 − 4126	IIIb	N*		—		
16029 − 3041	IIIb	D	24	AFGL1822		
16105 − 4205	VIb	D	25	OH/IR object		9
16114 − 5946	V	N		PK326-6.1		
16245 − 3859	V	N*		—		
16314 − 5611	IIIb	D		—		
16342 − 3814	V	N		High vel. OH maser		4
16416 − 2758	V	N		PK352+11.2		
16423 + 2353	V	N		PK43+37.1, NGC6210		
16456 − 3542	V	N*		PK347+5.1		1
16559 − 2957	IV	N*		—	F5	13
17026 − 4932	IIIb	N		—		
17028 − 1004	IV	N*	26	M2-9, PK10+18.2		
17047 − 5650	IV	D	24	CPD-568032	WC11	14
17180 − 2708	V	N*		519-PN 13 Pl		
17189 − 6501	IIIb	N		—		
17262 − 2343	V	N*		PK2+5.1		1
17267 − 1926	VIa	D*	23	TW Oph	Nb	15
17311 − 4924	V	D	21	CD − 4911554	Be	
17331 − 1618	IIIb	N		AFGL5369		
17436 + 5003	V	N	27	HD161796	F8	2
17531 − 0940	IIIb	N*		—		
17567 − 3849	V	N		PK352-07.1		
17584 + 6638	V	N		PK96+29.1		1,2
18081 − 0338	IV	N*		—		
18095 + 2704	V	N		—	F3	2,5
18096 + 0650	V	N		PK34+11.1, NGC6572		1,2
18129 − 3053	V	N		SwSt 1, PK1-6.2		1,2
18237 − 2408	IIIb	N*		—		
18281 + 2149	IIIb	N		AC Her, SAO86134	F8	
18298 − 2111	IIIb	N*		—		
18379 − 1707	V	N*		—		
18430 − 1430	V	N*		M1-61		
18467 − 4802	IIIb	D	24	—		
18491 − 3648	IIIb	N		—		
19016 − 2330	V	N		—		

TABLE 6. *(continued)*

Source	Region	Det[a]	Ref[b]	Identification	Sp.type	Ref[c]
19017 − 0545	VIa	D	23	V Aql	N6	15
19158 + 0141	V	N		PK37-5.1, V605 Aql		
19161 + 2343	IIIb	N	25	AFGL2362		
19178 − 2620	IIIb	D		AFGL2370		
19204 + 0124	IV	N*		PK37-6.1,NGC6790		1
19231 − 2717	VIb	N		—		
19288 + 2923	IIIb	N*		—, OH maser		10
19327 + 3024	IV	N		PK64+5.1		1
19434 + 5024	V	N		PK83+12.1,NGC6826		1
19500 − 1709	V	D	27	SAO163075	F8	2,6
20181 + 2234	IIIb	N*		— OH maser		10
20406 + 2953	V	N*				
21014 − 1133	V	N		PK37-34.1, NGC7009		1
21306 + 4422	V	?	26	PK89-5.1,IC5117		1,7
21399 + 3516	VIa	D	17	V460 Cyg	N1	15
21554 + 6204	IIIb	D	28	—		
22223 + 4327	V	?		—		
23234 + 4215	V	N		PK106-17.1, NGC7662		1,2
23268 + 6854	VIb	N	29	—		
23438 + 0312	VIa	D	23	TX Psc	N0	15
23541 + 7031	VIb	?*		PK118+18.1		

1. Zijlstra et al. (1989), 2. Volk & Kwok (1989), 3. Kwok et al. (1989), 4. te Lintel Hekkert et al. (1988), 5. Hrivnak et al. (1988), 6. Cernicharo et al. (1989), 7. Cohen & Schwarz (1984), 8. Beichman et al. (1986), 9. Gaylard et al. (1989), 10. te Lintel Hekkert et al. (1989), 11. Menzies & Wolstencroft (1990), 12. Hu et al. (1989), 13. Hu et al. (1990), 14. Rao et al. (1990), 15. Lambert et al. (1986), 16. Heske et al. (1990), 17. Olofsson et al. (1987), 18. Woodsworth et al. (1990), 19. Sopka et al. (1989), 20. Knapp & Morris (1985), 21. Loup et al. (1990), 22. Zuckerman et al. (1986), 23. Olofsson et al. (1988), 24. Knapp et al. (1989), 25. Zuckerman & Dyck (1986b), 26. Huggins & Healy (1989), 27. Likkel et al. (1987), 28. Zuckerman & Dyck (1986a), 29 Arquilla et al. (1986), 30. Pesce et al. (1988).

a. D = Detected by us, ? = Tentative detection, N = Non–detection, * = Interstellar line in the CO spectrum.
b. Reference to previous CO detection.
c. Reference to identification

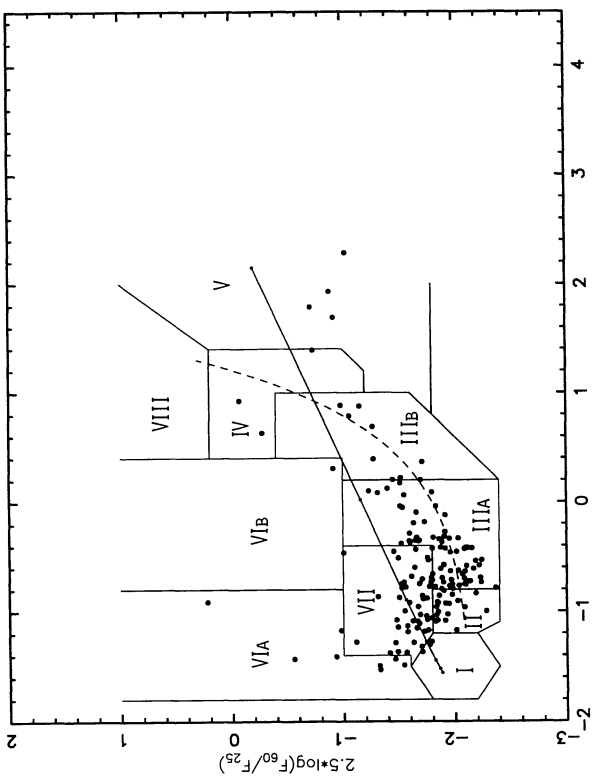

FIGURE 1c.

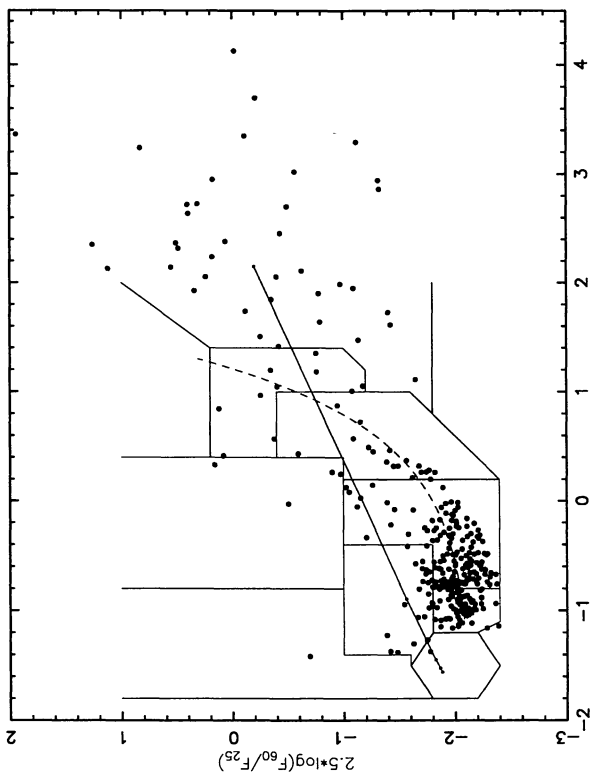

FIGURE 1d.

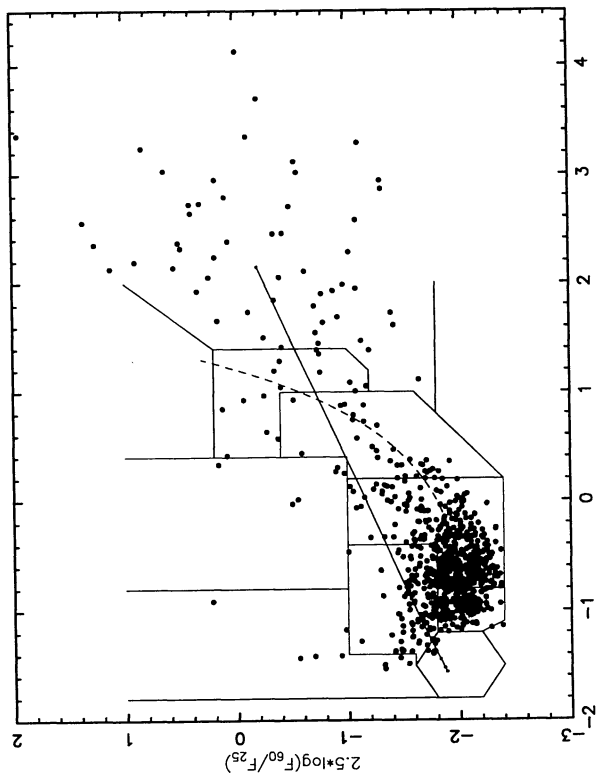

FIGURE 1a.

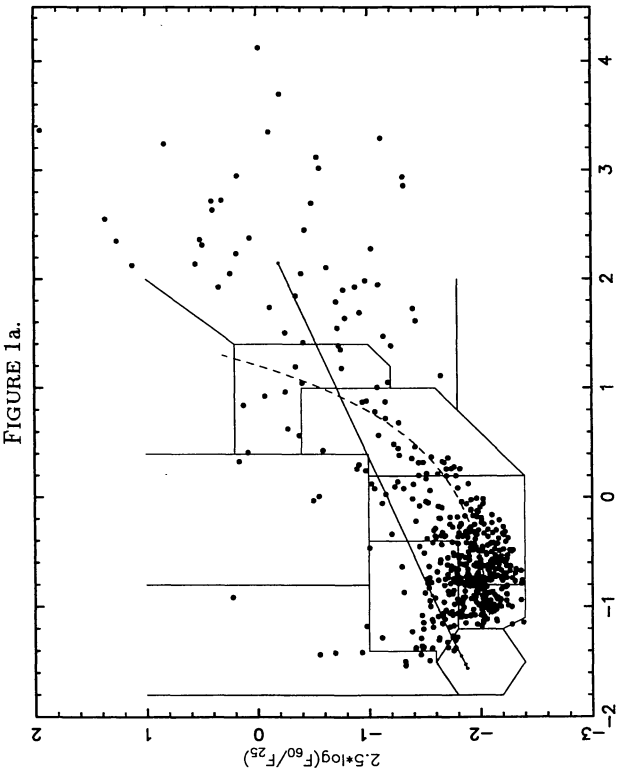

FIGURE 1b.

FIGURE 1a. The location of all objects in the sample in the IRAS two–color diagram. The 10 regions of van der Veen & Habing (1988), the black-body curve and the evolutionary sequence for O–rich stars (Bedijn, 1987) are included. b) The location of the objects in the observed part of the sample. c) The location of the detected sources. d) The location of the non–detected sources.

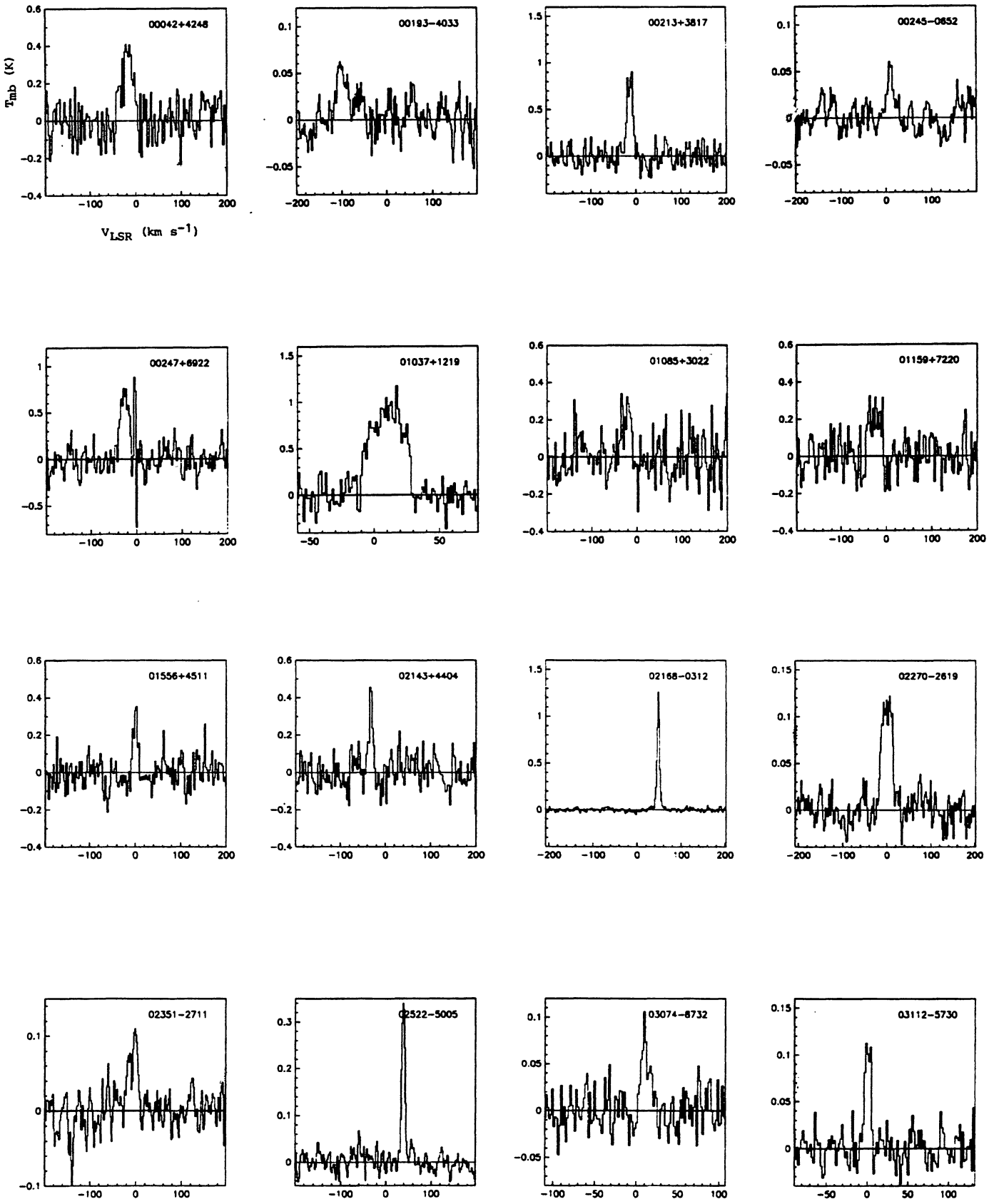

FIGURE 2. CO(1–0) spectra of all detected sources. The CO lines emanating from interstellar clouds in the line of sight have been cut in the spectra of IRAS09425-6040 and IRAS15148-4940, to better show the line profiles of the circumstellar CO emission.

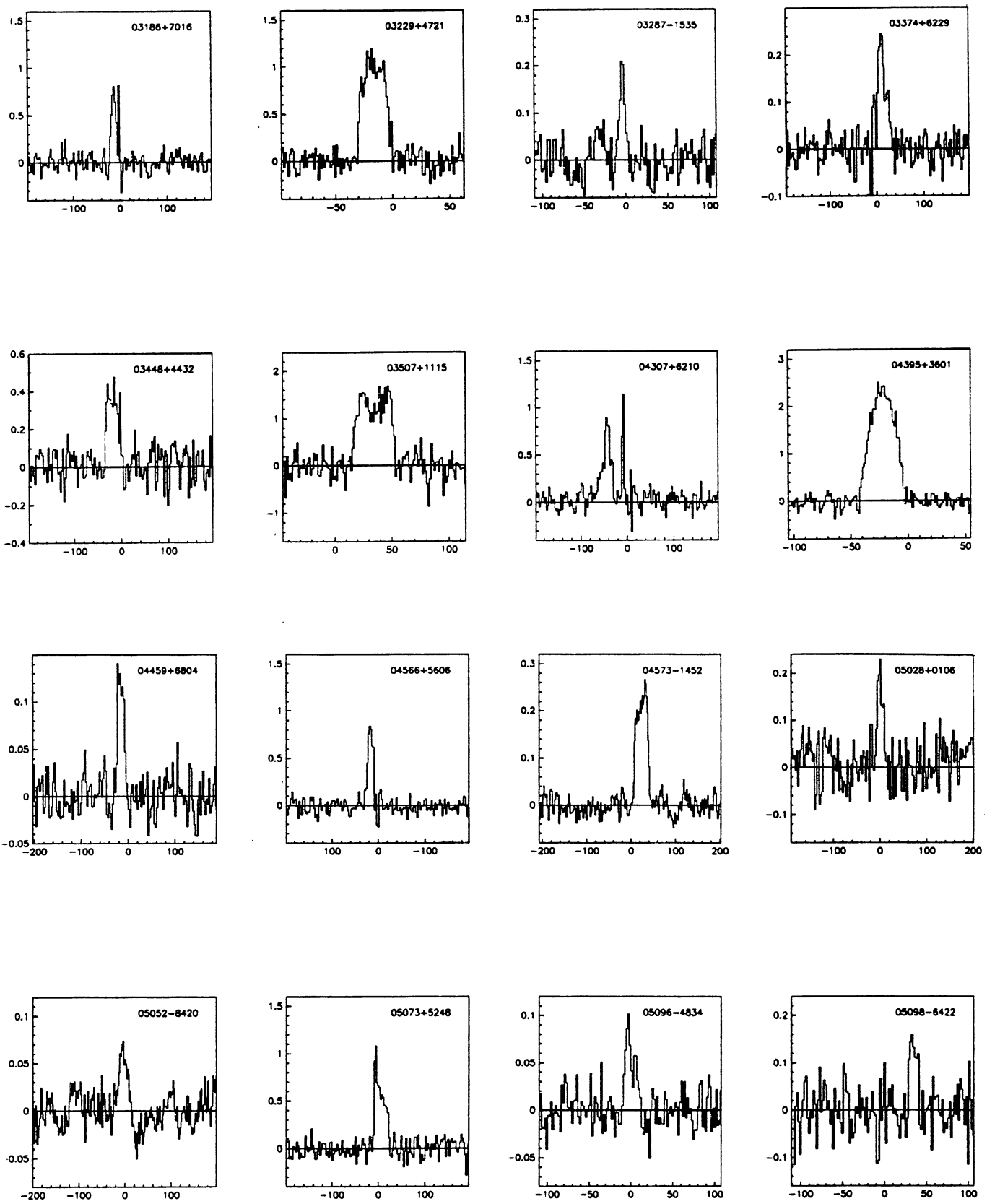

FIGURE 2. (continued)

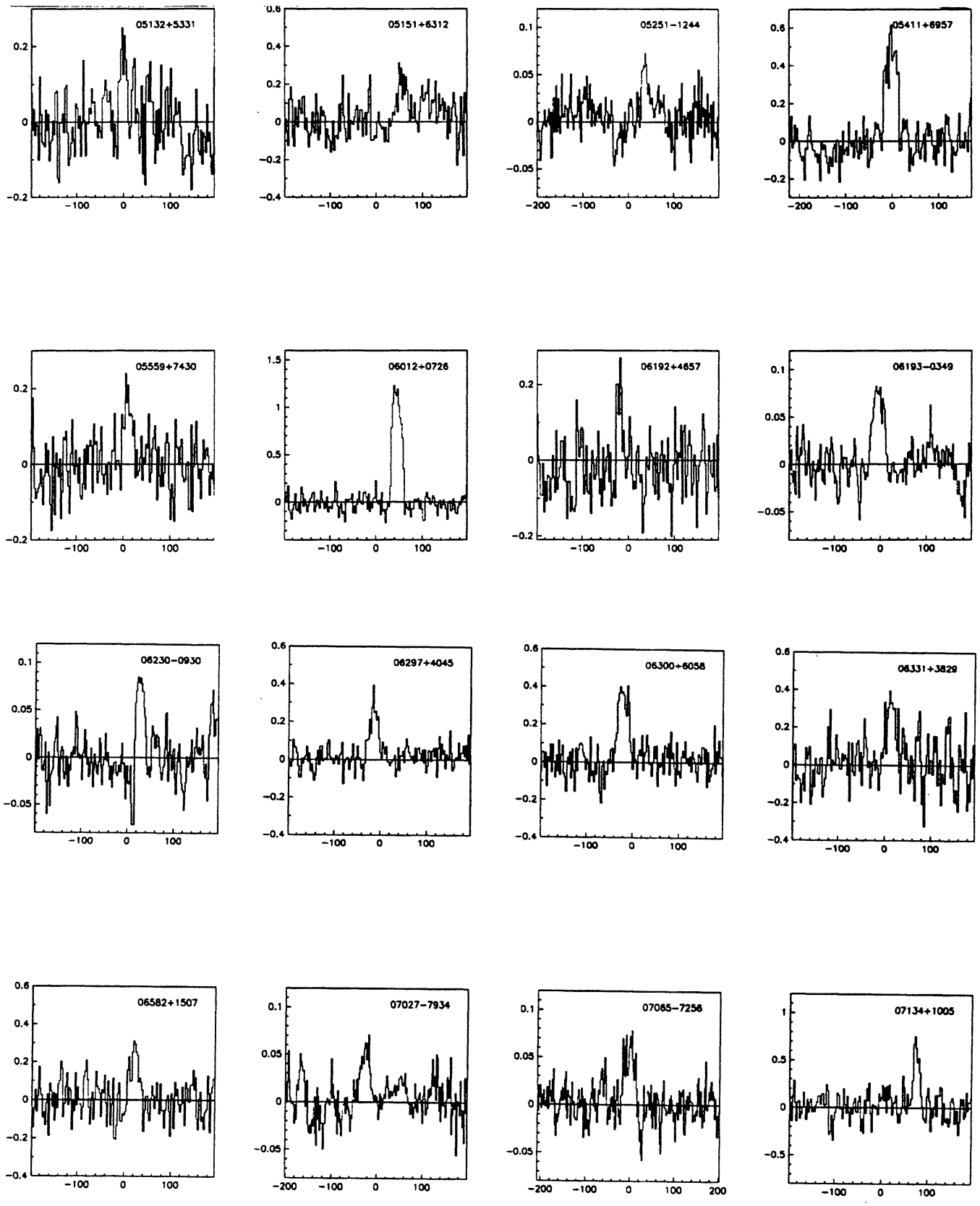

FIGURE 2. (continued)

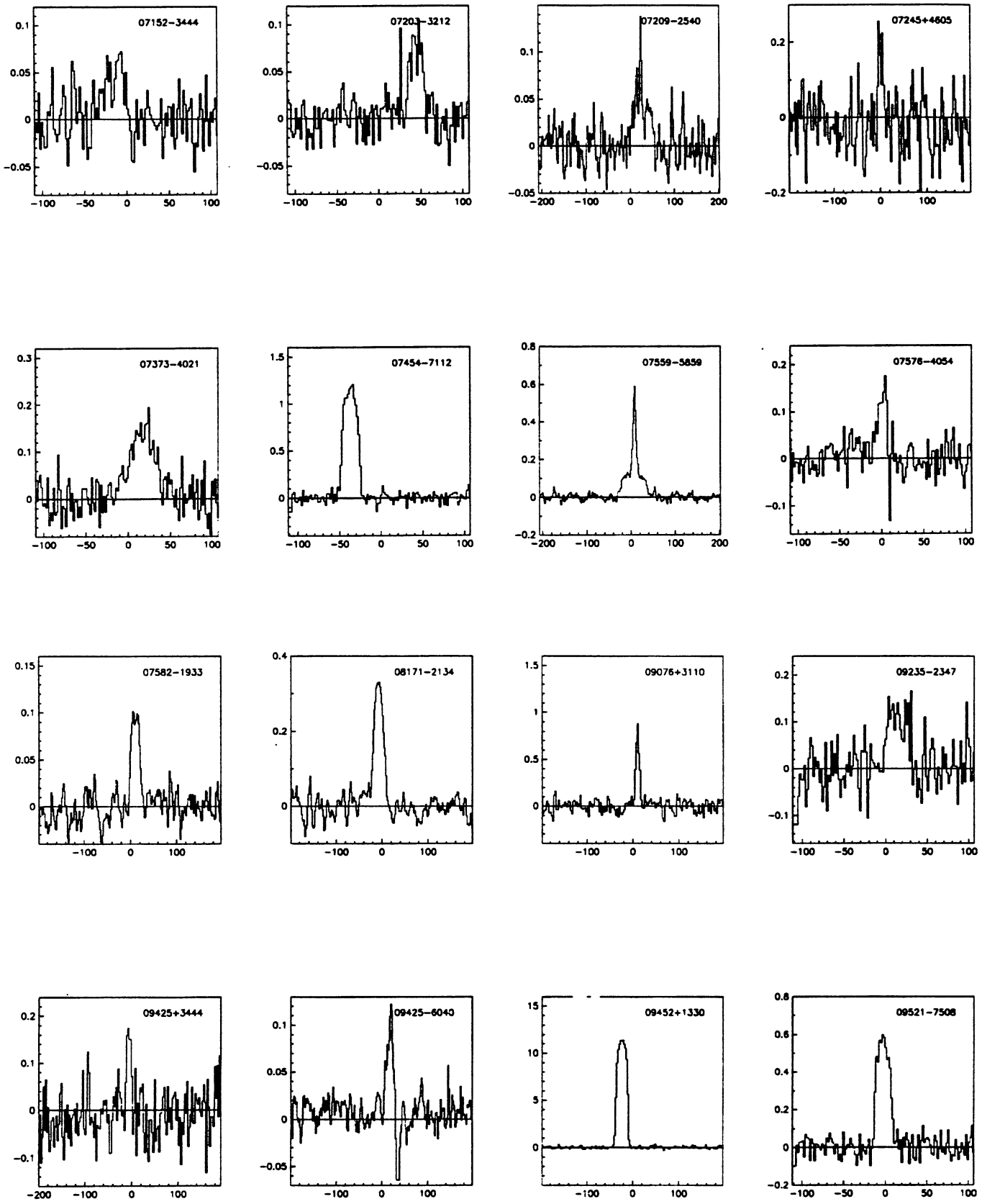

FIGURE 2. (continued)

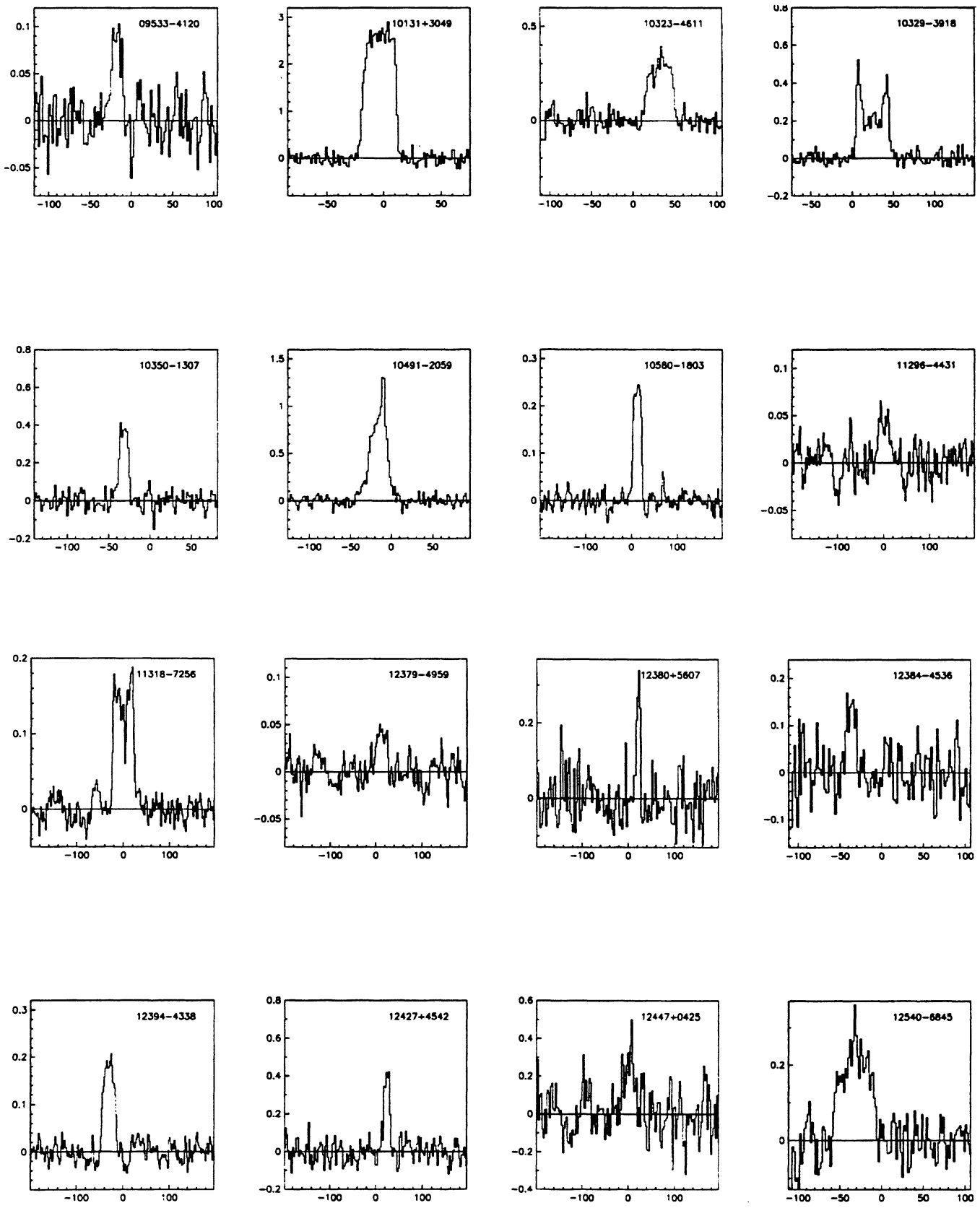

FIGURE 2. (continued)

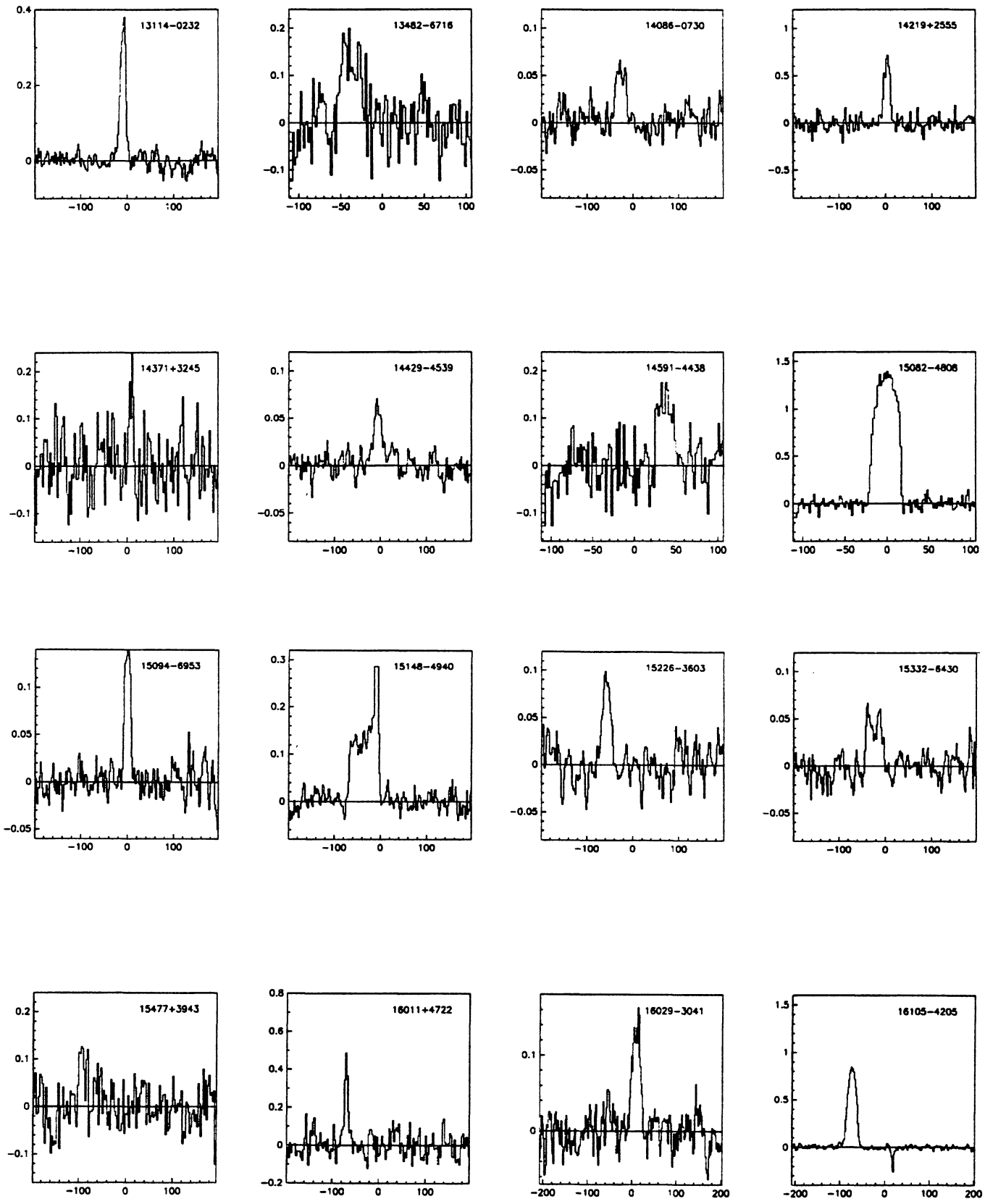

FIGURE 2. (continued)

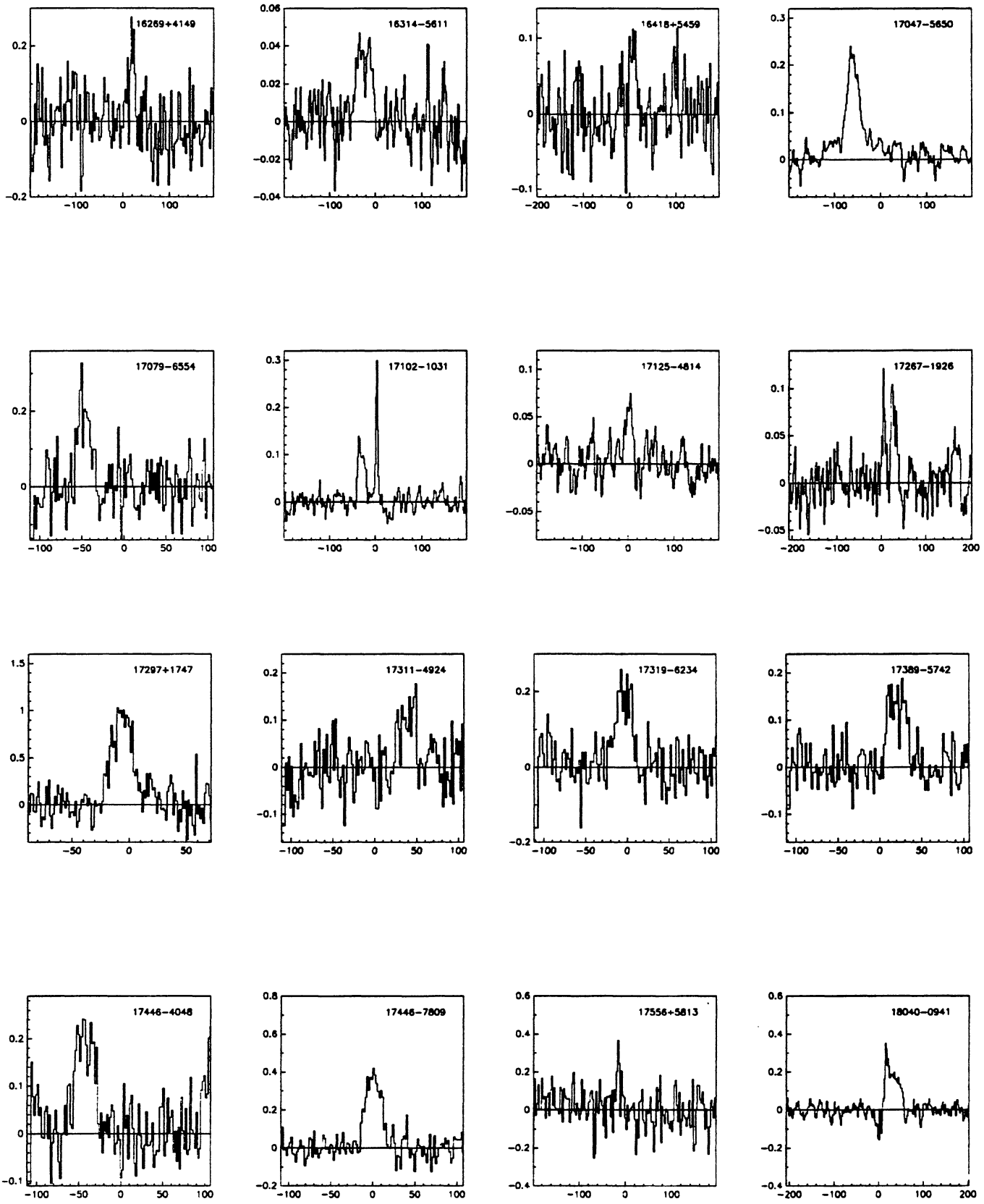

FIGURE 2. (continued)

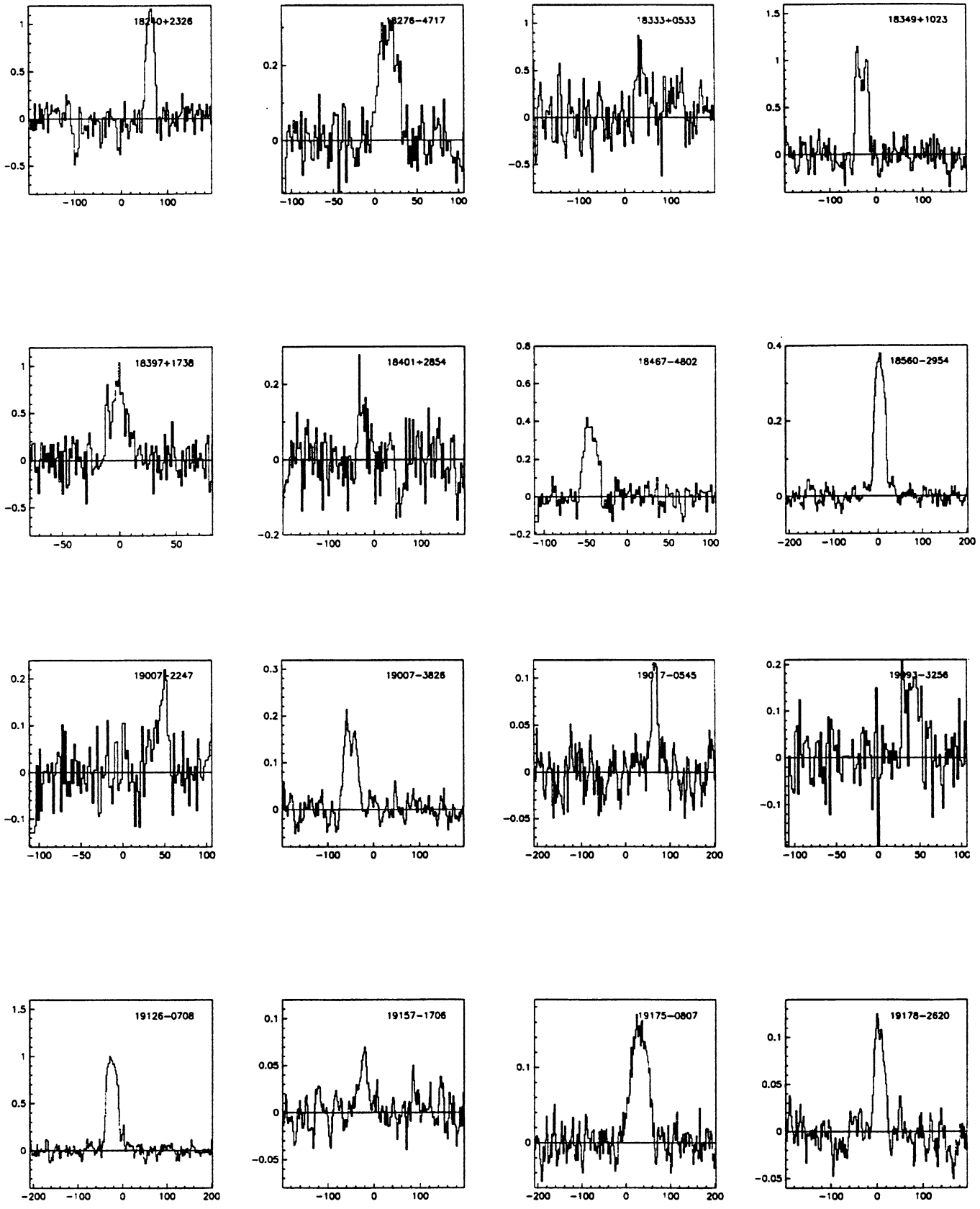

FIGURE 2. (continued)

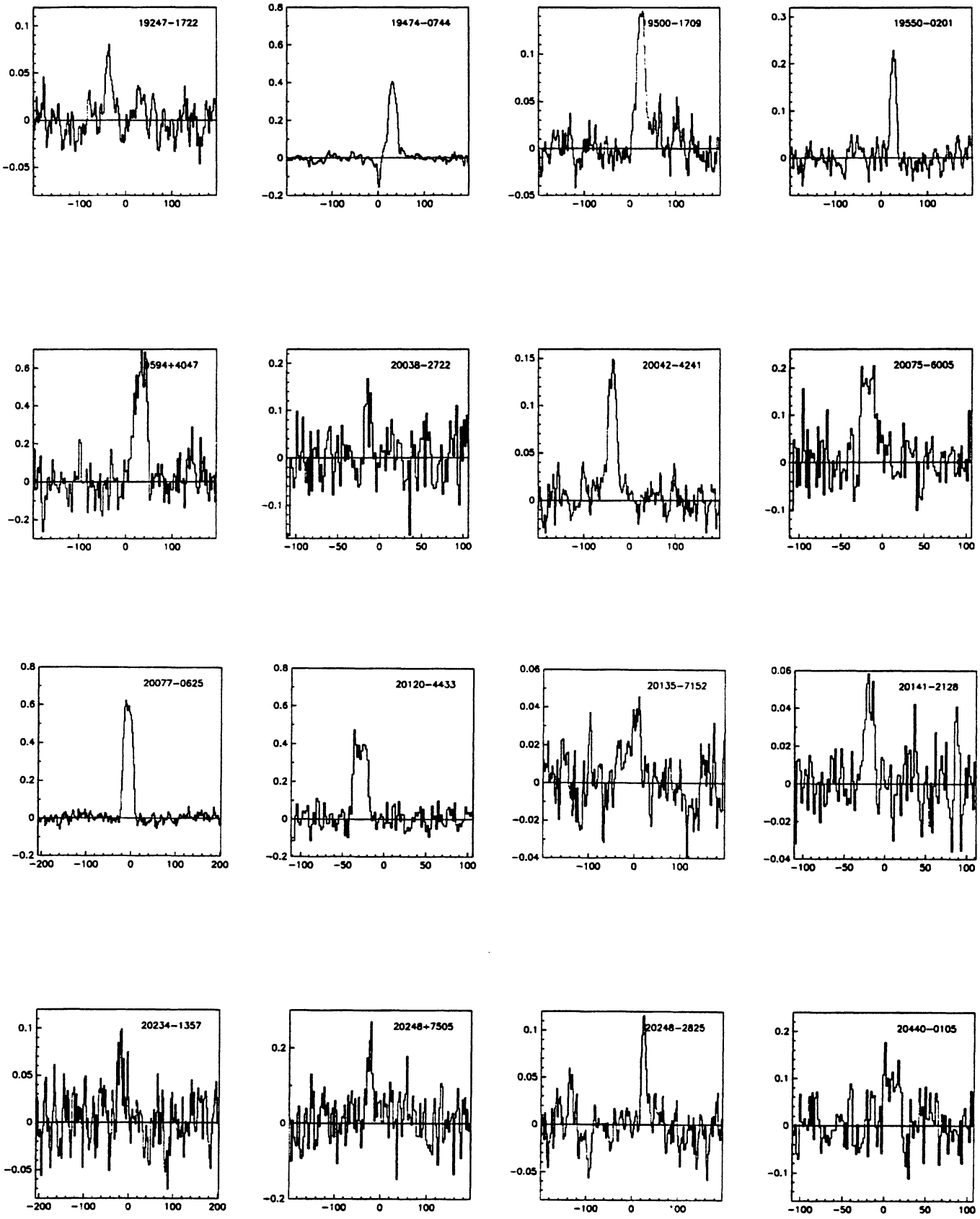

FIGURE 2. (continued)

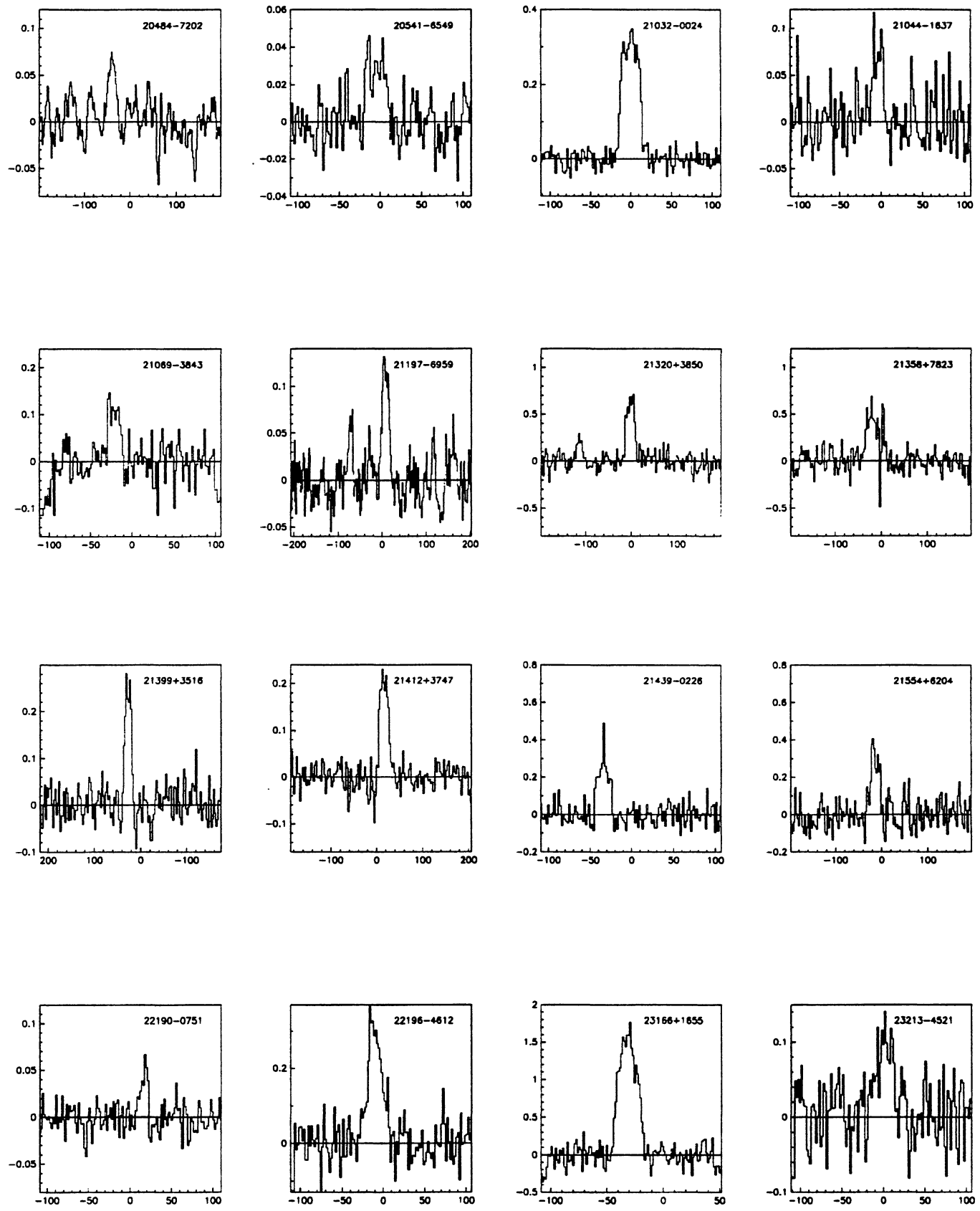

FIGURE 2. (continued)

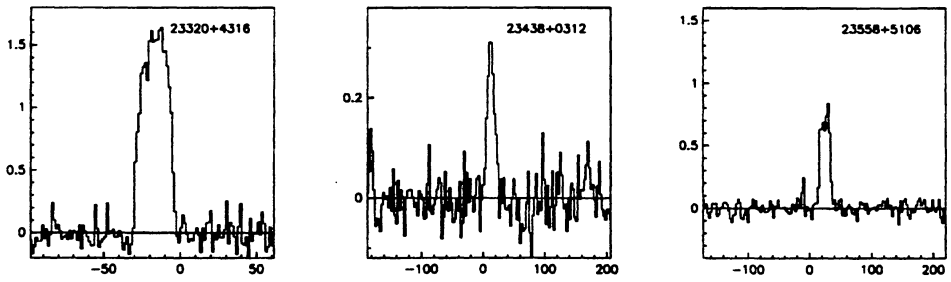

FIGURE 2. (continued)

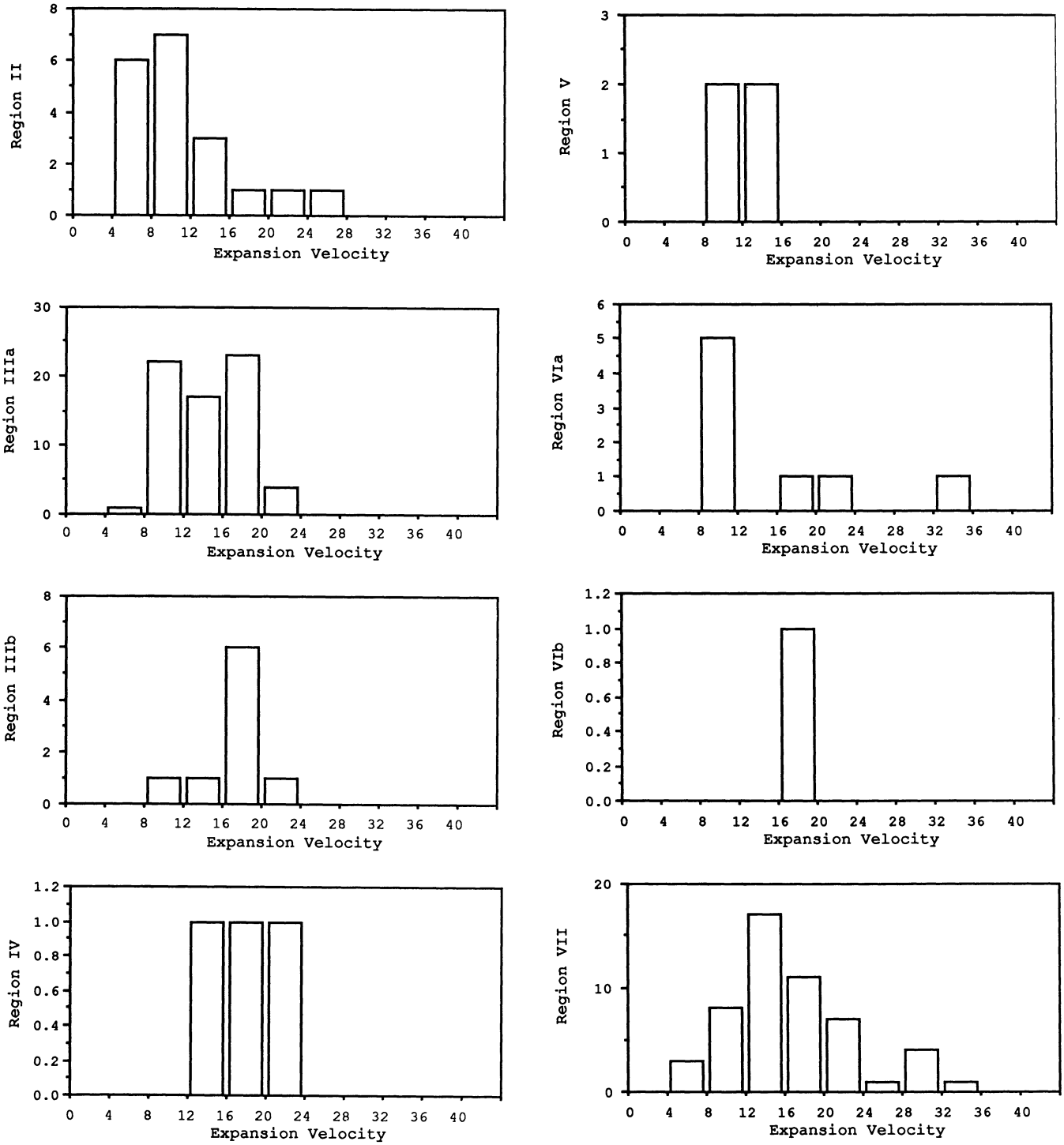

FIGURE 3. Histograms of the expansion velocities of the detected sources, divided into IRAS regions.

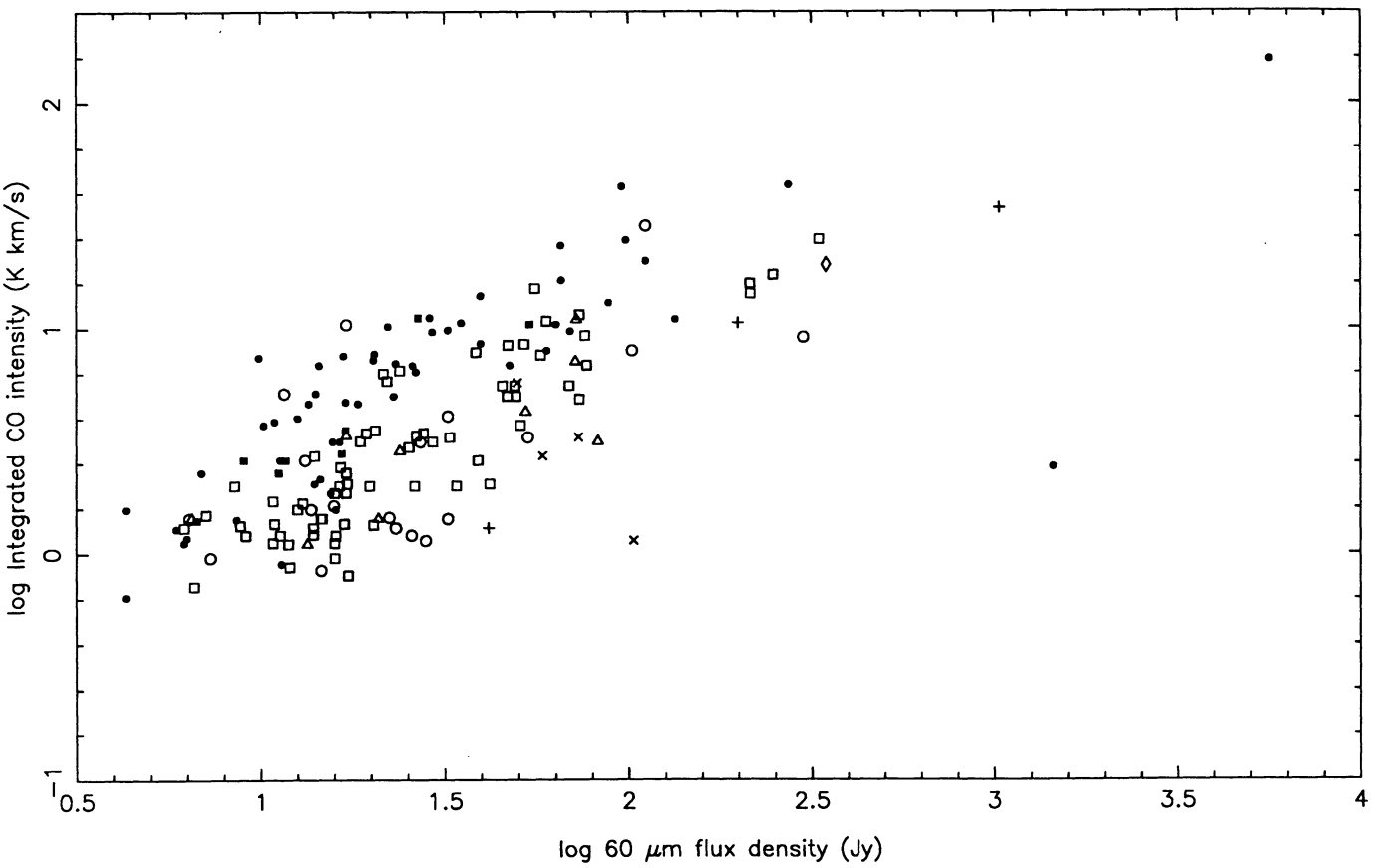

FIGURE 4. The integrated CO intensity (given in SEST main beam brightness intensity) as function of IRAS 60 μm flux density for the detected sources, plotted on a log–log scale. Note that region VIa and VII sources (mainly carbon-rich) on the average have higher integrated CO intensities than sources in the other regions. o = region II, □ = region IIIa, △ = region IIIb, + = region IV, × = region V, ▪ = region VIa, ◇ = region VIb, • = region VII.